Max-Planck-Institut
für Plasmaphysik

Overview of recent pedestal studies at ASDEX Upgrade

E. Wolfrum[1], E. Viezzer[1], A. Burckhart[1], M. G. Dunne[1], P. A. Schneider[1], M. Willensdorfer[1], E. Fable[1], R. Fischer[1], D. Hatch[3], F. Jenko[1], B. Kurzan[1], P. Manz[2], S. K. Rathgeber[1] and the ASDEX Upgrade Team

[1]Max-Planck-Institut für Plasmaphysik, Garching, Germany
[2]Physik-Department E28, Technische Universität München, Garching, Germany
[3]Institute for Fusion Studies, University of Texas at Austin, Austin, Texas, USA

This work has been carried out within the framework of the EUROfusion Consortium and has received funding from the European Union's Horizon 2020 research and innovation programme under grant agreement number 633053. The views and opinions expressed herein do not necessarily reflect those of the European Commission.

Motivation

- When entering the H-mode an edge transport barrier evolves
  → pedestal

- ∇p not stable: edge localised modes limit pedestal height and width

Aim: Identification of dominant transport mechanisms in the pedestal

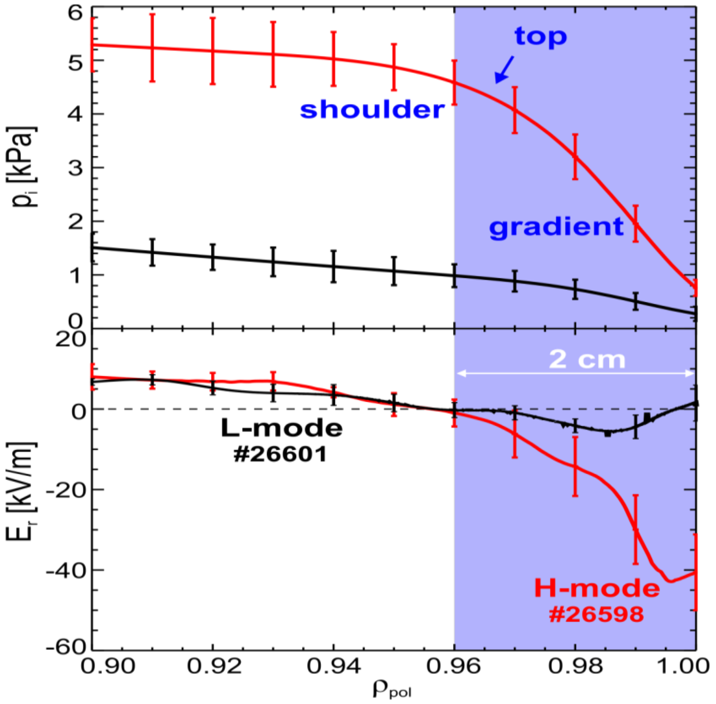

Outline

- New and upgraded diagnostics at ASDEX Upgrade
- Particle transport analysis after L-H transition
- Neoclassical nature of E_r, impurity flows and j
- ELM cycle studies
  - Peeling-ballooning stability analysis
  - Gyrokinetic analysis
- Summary and Conclusions

Outline

- New and upgraded diagnostics at ASDEX Upgrade
- Particle transport analysis after L-H transition
- Neoclassical nature of E_r, impurity flows and j
- ELM cycle studies
  - Peeling-ballooning stability analysis
  - Gyrokinetic analysis
- Summary and Conclusions

Diagnostic capabilities for measuring the pedestal structure at AUG

- Radial profiles of T_e, n_e, T_i
  $\tilde{T}_e$, $\tilde{n}_e$
- HFS/LFS flows and E_r
- j via pressure constrained equilibrium
- Integrated Data Analysis (IDA):
  n_e, T_e combining several diagnostics
  e.g. new forward model of ECE radiation transport

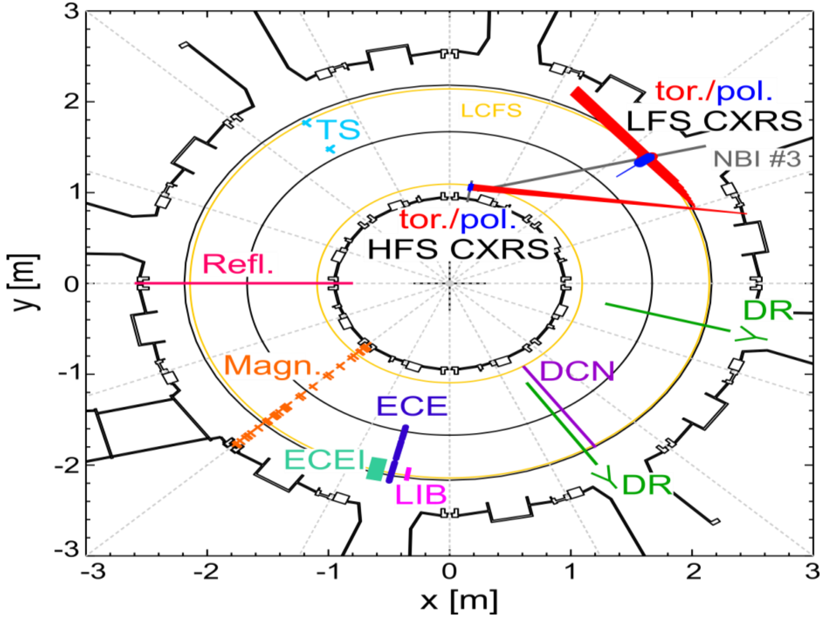

M. G. Dunne *et al*, NF **52** 123014 (2012)
R. Fischer *et al*, FST 58 675 (2010)
S. K. Rathgeber *et al*, PPCF **55** 025004 (2013)
E. Viezzer *et al*, RSI **52** 123014 (2012)

Overview of turbulence studies: see U. Stroth, EX/11-1

Highly resolved edge profiles allow for unprecedented comparison between experiment & theory

- High-accuracy localization of T_e, n_e, T_i, v_{rot}, j and E_r with respect to LCFS position
- Upgraded and new diagnostics enable detailed study of pedestal structure and stability using linear MHD modelling and GK simulations

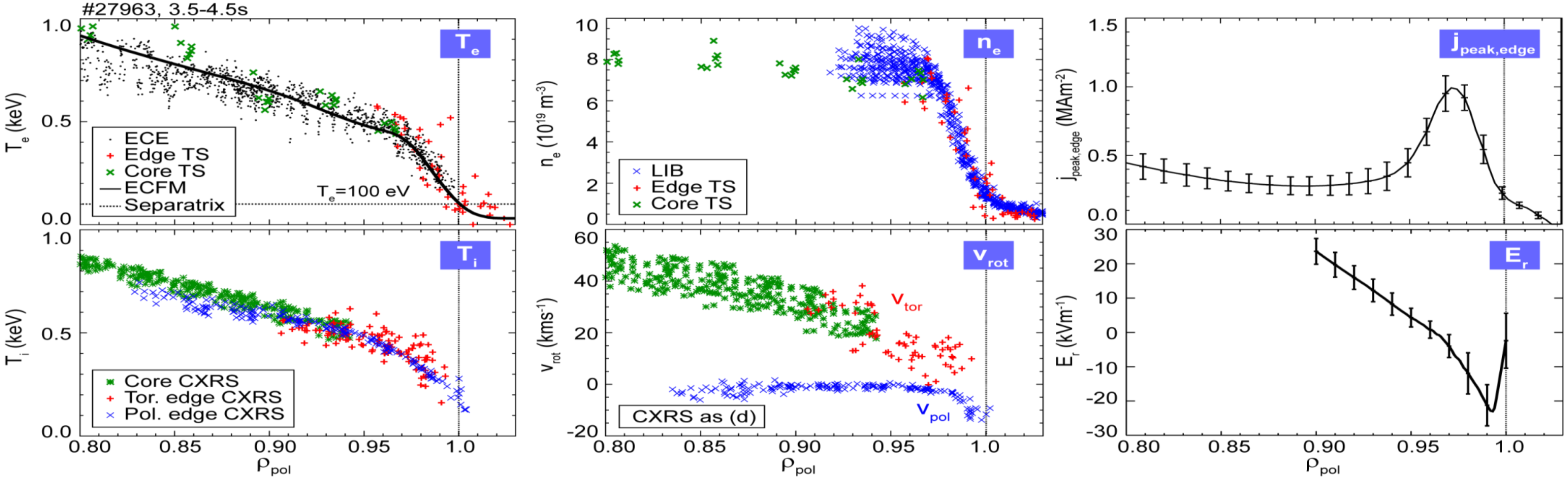

Outline

- New and upgraded diagnostics at ASDEX Upgrade
- Particle transport analysis after L-H transition
- Neoclassical nature of E_r, impurity flows and j
- ELM cycle studies
  - Peeling-ballooning stability analysis
  - Gyrokinetic analysis
- Summary and Conclusions

Temporal development of density build-up is modelled with ASTRA*

- Is the particle ETB due to a particle pinch v_e or a reduction of diffusion D?

$$\boxed{\frac{\partial n_e}{\partial t}} + \frac{1}{r}\frac{\partial}{\partial r} r\left(-\boxed{D}\,\boxed{\frac{\partial n_e}{\partial r}} + \boxed{v_e}\,\boxed{n_e}\right) = \boxed{S}$$

- Extensive parameter scan in D, v_e, S
  (D_{edge} = 0.001 – 10 m^2/s)
  (v_{edge} = 0 – 100 m/s)
  (via neutral gas density $n_0 = 10^{15} – 10^{18}$ m^{-3})

- Comparison of temporal evolution of ASTRA density with measured n_e

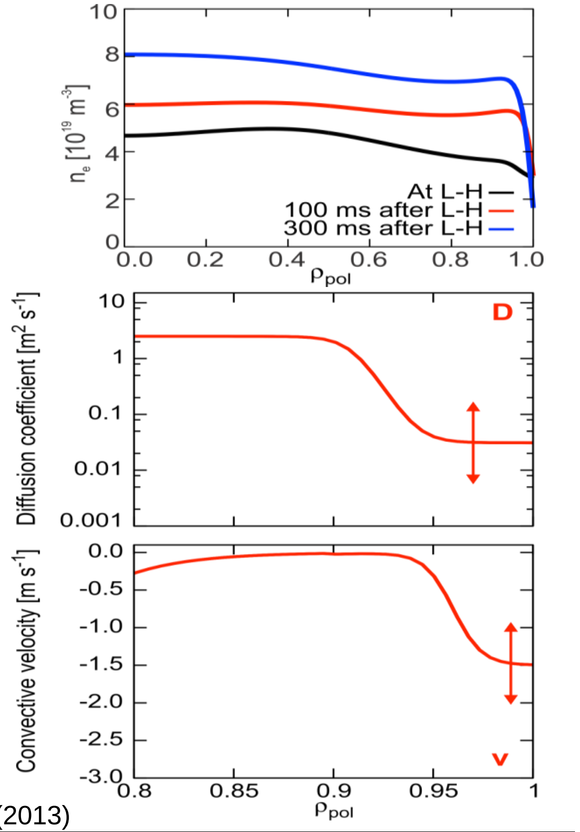

*G. V. Pereverzev *et al*, IPP 5/42 (1991)

M. Willensdorfer *et al*, NF **53** 0930201 (2013)

Density build-up can be reproduced by assuming purely diffusive ETB

- Diffusive ETB is needed to reproduce n_e build-up after L-H transition (D_{edge} ~ 0.037 m^2/s)
- Particle pinch cannot replace diffusive ETB
- Small pinch (~ 0.4 m/s) in addition to diffusive ETB enhances simulation

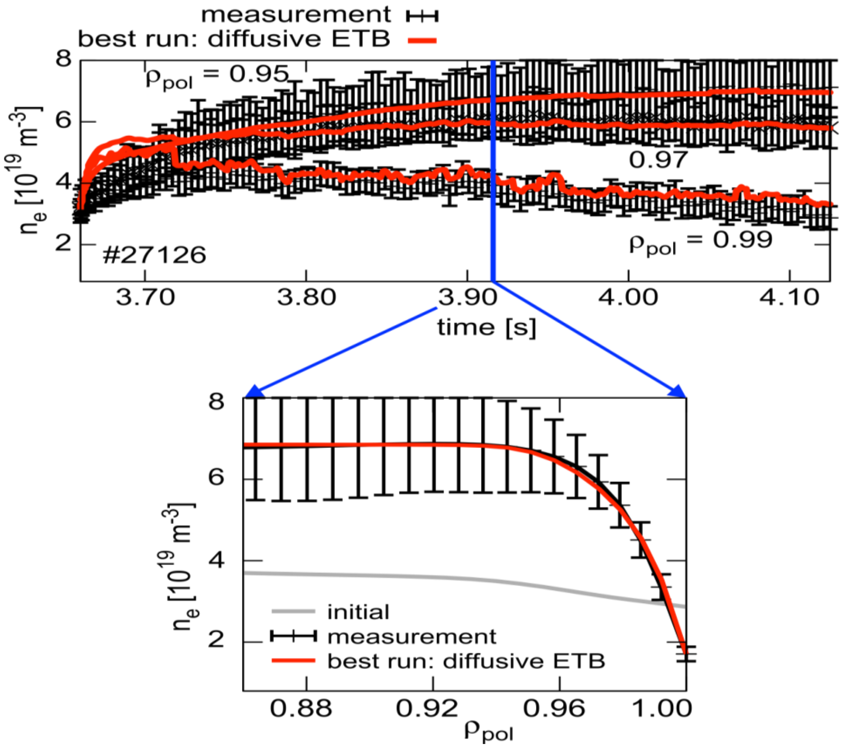

M. Willensdorfer *et al*, NF **53** 0930201 (2013)

Outline

- New and upgraded diagnostics at ASDEX Upgrade
- Particle transport analysis after L-H transition
- Neoclassical nature of E_r, impurity flows and j
- ELM cycle studies
  - Peeling-ballooning stability analysis
  - Gyrokinetic analysis
- Summary and Conclusions

Evidence for neoclassical nature of E_r

- CXRS measurements allow for detailed study of E_r and edge ion and electron profiles

- Poloidal rotation velocity is at neoclassical level → neoclassical nature of E_r in pedestal, $E_r \approx \nabla p_i / e n_i$

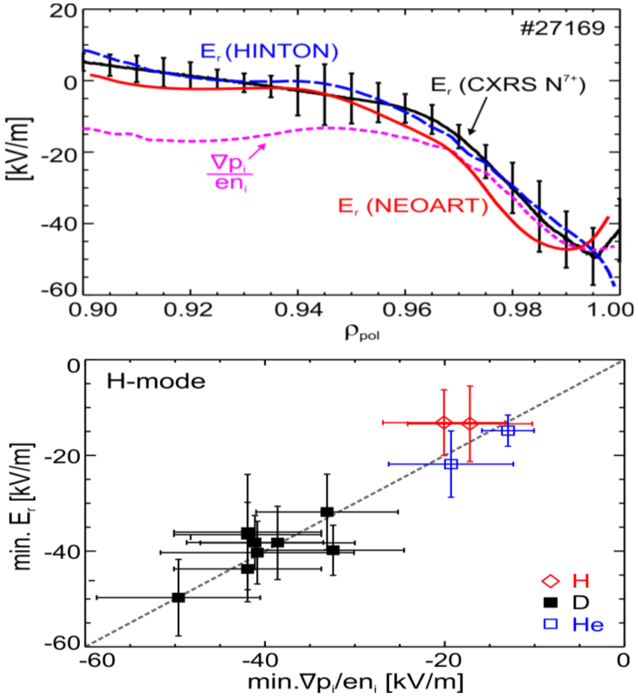

E. Viezzer *et al*, NF **54** 012003 (2014)
R. M. McDermott *et al*, PoP **16** 056103 (2009)
E. Viezzer *et al*, PPCF **56** 075018 (2014)

Evidence for neoclassical nature of E_r

- CXRS measurements allow for detailed study of E_r and edge ion and electron profiles
- Poloidal rotation velocity is at neoclassical level → neoclassical nature of E_r in pedestal, $E_r \approx \nabla p_i / e n_i$
- High-accuracy localization technique revealed that maximum $\omega_{E\times B}$ and steepest ∇p_i align with negative E_r shear region

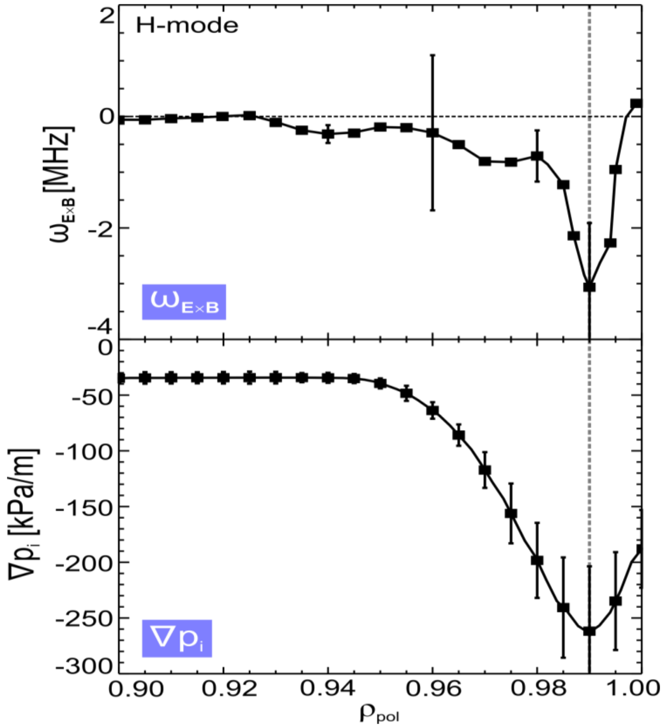

E. Viezzer *et al*, NF **54** 012003 (2014)
R. M. McDermott *et al*, PoP **16** 056103 (2009)
E. Viezzer *et al*, PPCF **56** 075018 (2014)

Evidence for neoclassical nature of E_r

- CXRS measurements allow for detailed study of E_r and edge ion and electron profiles
- Poloidal rotation velocity is at neoclassical level → neoclassical nature of E_r in pedestal, $E_r \approx \nabla p_i / e n_i$
- High-accuracy localization technique revealed that maximum $\omega_{E\times B}$ and steepest ∇p_i align with negative E_r shear region

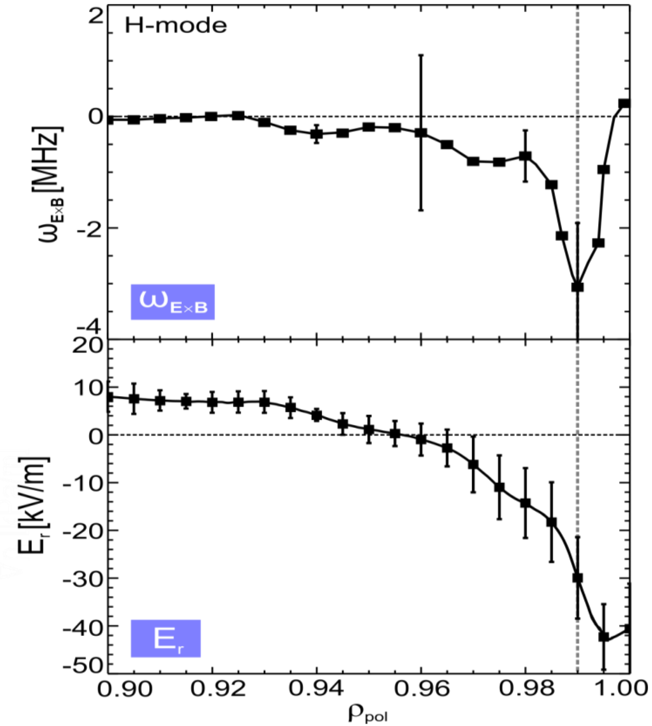

E. Viezzer *et al*, NF **54** 012003 (2014)
R. M. McDermott *et al*, PoP **16** 056103 (2009)
E. Viezzer *et al*, PPCF **56** 075018 (2014)

Asymmetry in flow structure consistent with divergence-free flows

- HFS/LFS CXRS demonstrate existence of in-out impurity density asymmetry in ETB → asymmetric flow structure on flux surface consistent with $\nabla\cdot(n_\alpha v_\alpha) = 0$

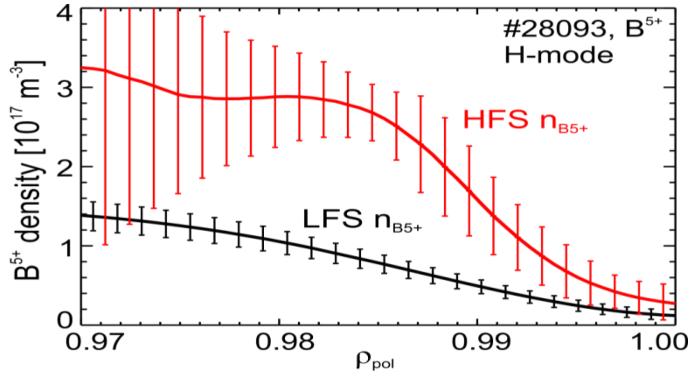

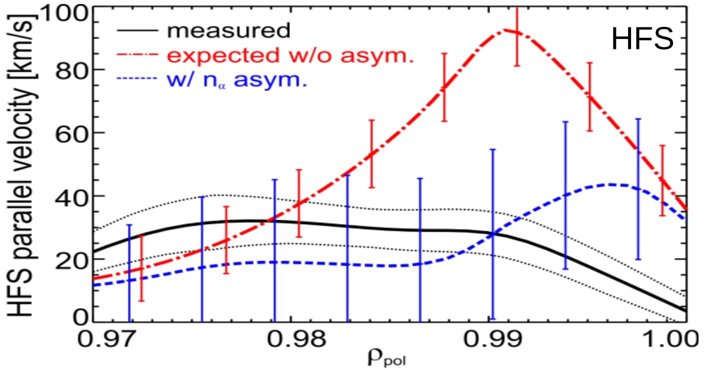

E. Viezzer *et al*, PPCF **55** 124037 (2013)
T. Pütterich *et al*, NF **52** 083013 (2012)

Asymmetry in flow structure consistent with divergence-free flows

- HFS/LFS CXRS demonstrate existence of in-out impurity density asymmetry in ETB → asymmetric flow structure on flux surface consistent with $\nabla\cdot(n_\alpha v_\alpha) = 0$

- Fluid model based on parallel momentum balance including all terms → friction and poloidal centrifugal force (CF) are dominant driving terms close to LCFS

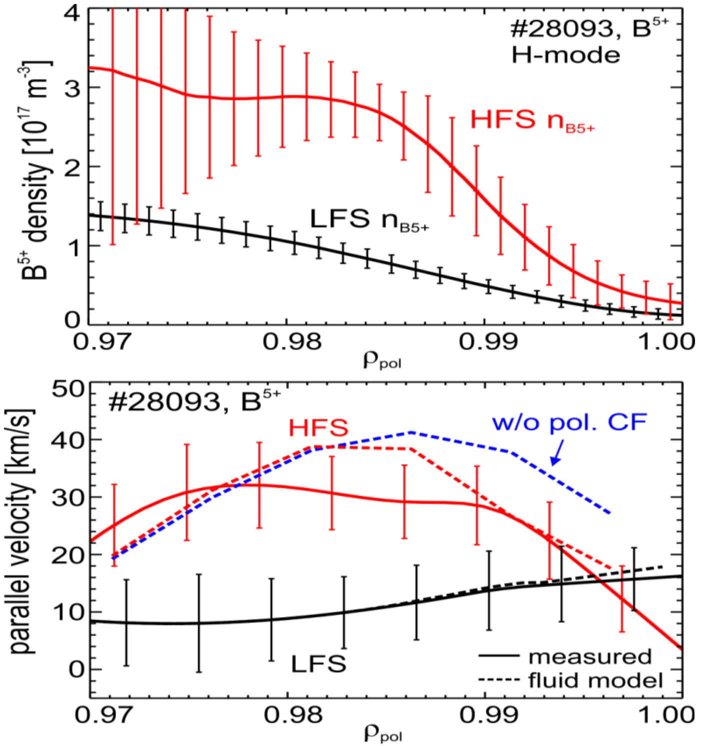

E. Viezzer *et al*, PPCF **55** 124037 (2013)
T. Pütterich *et al*, NF **52** 083013 (2012)

Asymmetry in flow structure consistent with divergence-free flows

- HFS/LFS CXRS demonstrate existence of in-out impurity density asymmetry in ETB → asymmetric flow structure on flux surface consistent with $\nabla\cdot(n_\alpha v_\alpha) = 0$

- Fluid model based on parallel momentum balance including all terms → friction and poloidal centrifugal force (CF) are dominant driving terms close to LCFS

- Only small influence on neoclassical impurity transport (v/D)

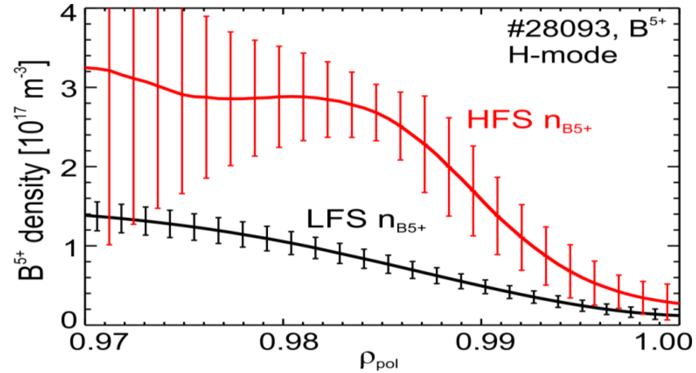

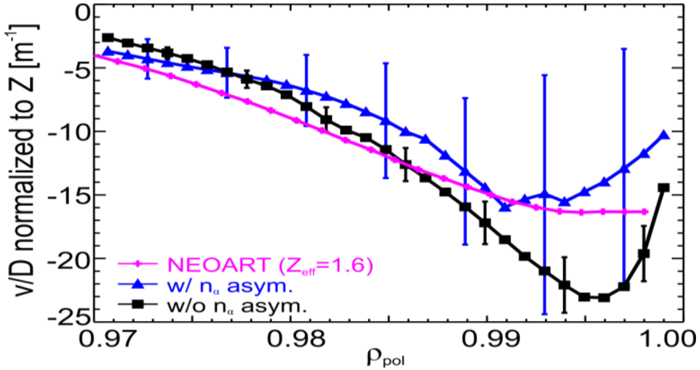

E. Viezzer *et al*, PPCF **55** 124037 (2013)
T. Pütterich *et al*, NF **52** 083013 (2012)

Edge current density is neoclassical

- Assume current driven by neoclassical bootstrap* and Ohmic current, neglect fast ion current, $\langle j_{PS}\cdot B\rangle = 0$

$$\boxed{\langle j_{\mathrm{neo}} \cdot B\rangle = \langle j_{\mathrm{boot}} \cdot B\rangle + \langle j_{\mathrm{Ohm}} \cdot B\rangle}$$

- Comparison of current density (CLISTE) to neoclassical prediction shows quantitative agreement

- Position and peak match, good agreement also during ELM cycle

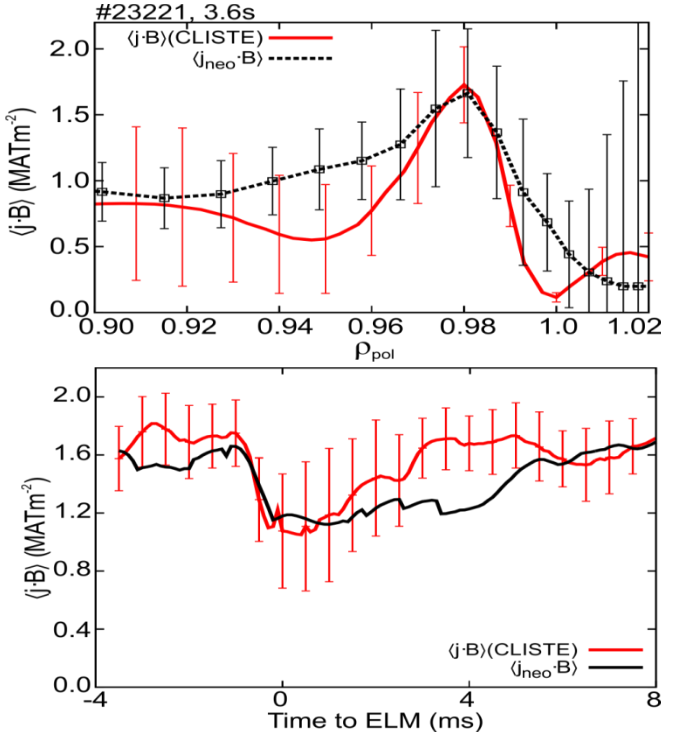

M. G. Dunne *et al*, NF **52** 123014 (2012)
P. J. McCarthy *et al*, PPCF **54** 015010 (2012)

*O. Sauter *et al*, PoP **6** 2834 (1999)

Outline

- New and upgraded diagnostics at ASDEX Upgrade
- Particle transport analysis after L-H transition
- Neoclassical nature of E_r, impurity flows and j
- ELM cycle studies
  - Peeling-ballooning stability analysis
  - Gyrokinetic analysis
- Summary and Conclusions

T_e and n_e profiles evolve separately during ELM cycle

- ELM cycle studies reveal different recovery timescales of T_e and n_e

- ∇T_e recovery shows 5 phases:
  (i) ∇T_e small during ELM
  (ii) initial ∇T_e recovery
  (iii) ∇T_e recovery stalls, ∇n_e recovers rapidly
  (iv) fast ∇T_e recovery continues, while ∇n_e stays constant
  (v) ∇T_e slowly evolving, both exhibit large fluctuations

- Behaviour is observed in all analyzed discharges, at all gas fueling levels

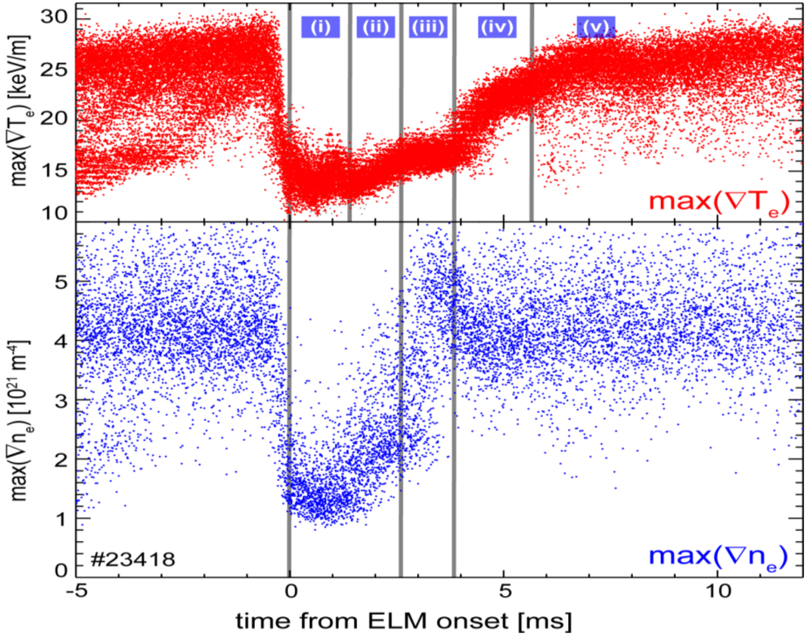

A. Burckhart *et al*, PPCF **52** 105010 (2010)

Gradual recovery of pressure gradient and current density during ELM cycle

- Before ELM crash (i)+(vi): j and ∇p constant
- After ELM crash (ii): j and ∇p recover gradually as ∇n_e builds up (iii), followed by build-up of ∇T_e (iv)
- Towards end of ELM cycle (v):
  j saturates as soon as ∇p saturates → pedestal is clamped at critical gradient before ELM crash

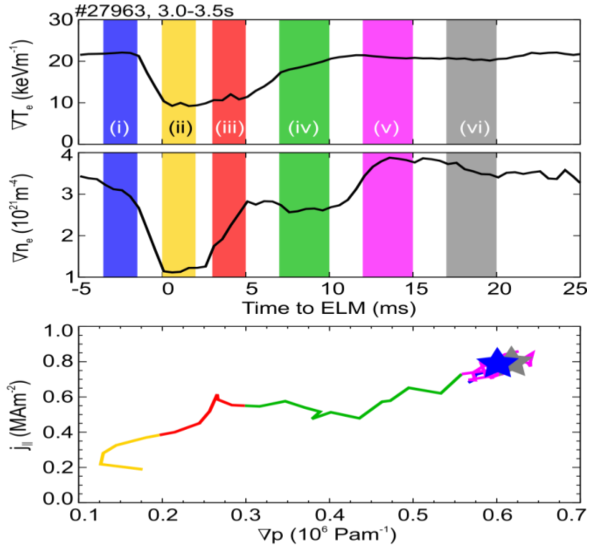

P. B. Snyder *et al*, PoP 19 056115 (2012)   D. Dickinson *et al*, PPCF **53** 115010 (2011)   A. Burckhart, PhD thesis, LMU Munich 2013

Peeling-ballooning stability analysis during ELM cycle

- Before ELM crash (i)+(vi): j and ∇p constant
- After ELM crash (ii): j and ∇p recover gradually as ∇n_e builds up (iii), followed by build-up of ∇T_e (iv)
- Towards end of ELM cycle (v):
  j saturates as soon as ∇p saturates $\rightarrow$ pedestal is clamped at critical gradient before ELM crash
- Towards end of ELM cycle stability boundary moves closer to op. point because pedestal width grows
- Final ELM trigger not determined by linear MHD stability alone (op. point ~30% lower than boundary)
- Other cases do show agreement with PB model

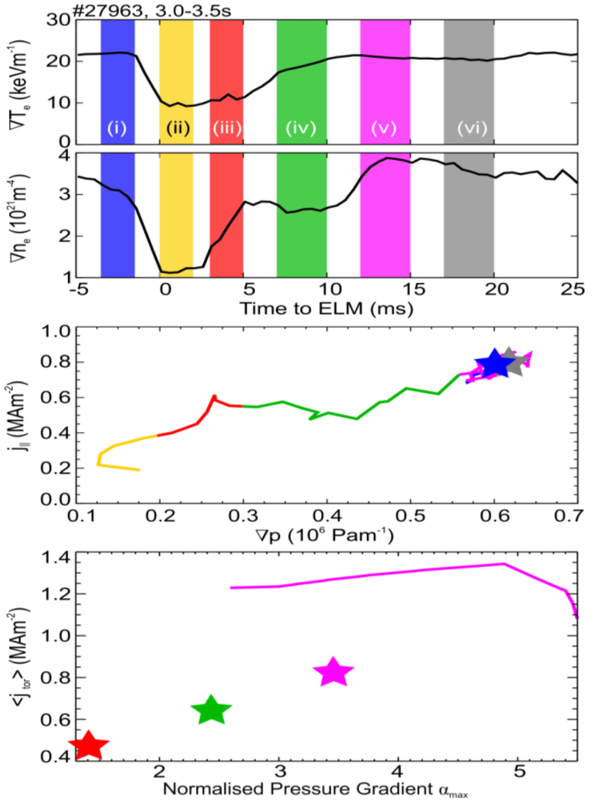

P. B. Snyder *et al*, PoP 19 056115 (2012) D. Dickinson *et al*, PPCF **53** 115010 (2011) A. Burckhart, PhD thesis, LMU Munich 2013

Peeling-ballooning stability analysis during ELM cycle

- Before ELM crash (i)+(vi): j and ∇p constant
- After ELM crash (ii): j and ∇p recover gradually as ∇n_e builds up (iii), followed by build-up of ∇T_e (iv)
- Towards end of ELM cycle (v): j saturates as soon as ∇p saturates → pedestal is clamped at critical gradient before ELM crash
- Towards end of ELM cycle stability boundary moves closer to op. point because pedestal width grows
- Final ELM trigger not determined by linear MHD stability alone (op. point ~30% lower than boundary)
- Other cases do show agreement with PB model

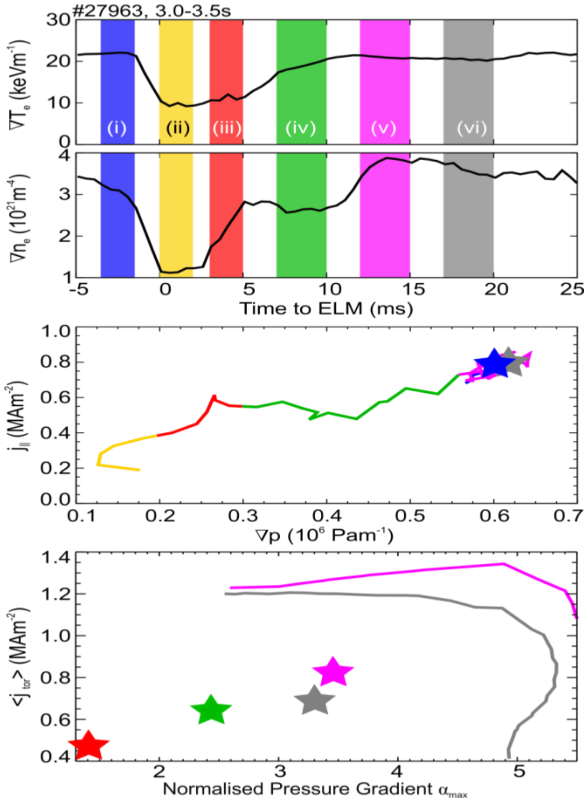

P. B. Snyder *et al*, PoP 19 056115 (2012) D. Dickinson *et al*, PPCF **53** 115010 (2011) A. Burckhart, PhD thesis, LMU Munich 2013

Peeling-ballooning stability analysis during ELM cycle

- Before ELM crash (i)+(vi): j and ∇p constant
- After ELM crash (ii): j and ∇p recover gradually as ∇n_e builds up (iii), followed by build-up of ∇T_e (iv)
- Towards end of ELM cycle (v):
  j saturates as soon as ∇p saturates → pedestal is clamped at critical gradient before ELM crash
- Towards end of ELM cycle stability boundary moves closer to op. point because pedestal width grows
- Final ELM trigger not determined by linear MHD stability alone (op. point ~30% lower than boundary)
- Other cases do show agreement with PB model

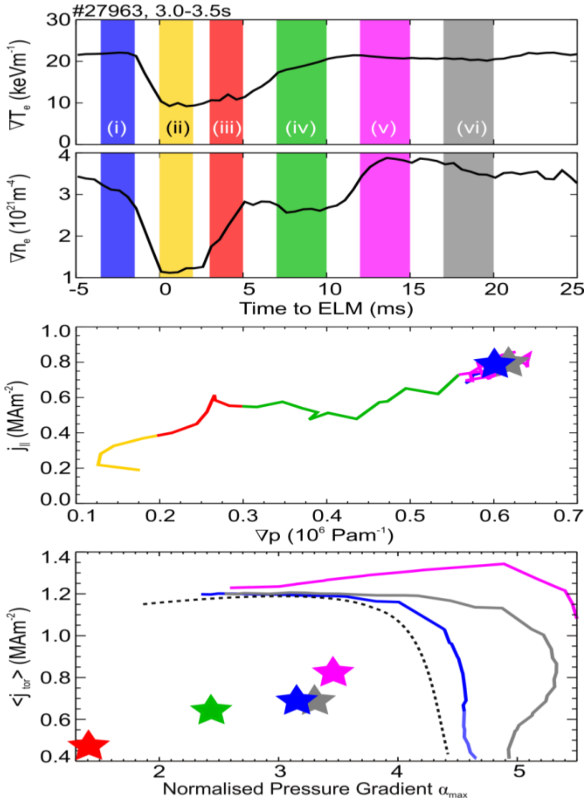

P. B. Snyder *et al*, PoP 19 056115 (2012) D. Dickinson *et al*, PPCF **53** 115010 (2011) A. Burckhart, PhD thesis, LMU Munich 2013

ECE-Imaging indicates presence of MTMs on pedestal shoulder

- For slow type-I ELMs 2D ECEI reveals occurrence of off-midplane T_e fluctuations on pedestal top, followed by mode at onset of ELM crash

- Both modes move in electron diamagnetic direction

- Velocimetry analysis:
  At ρ_{pol}~0.95 cross-phase between T_e and v_r fluctuations is ~ $\pi/2 \rightarrow$ points to MTMs on pedestal top

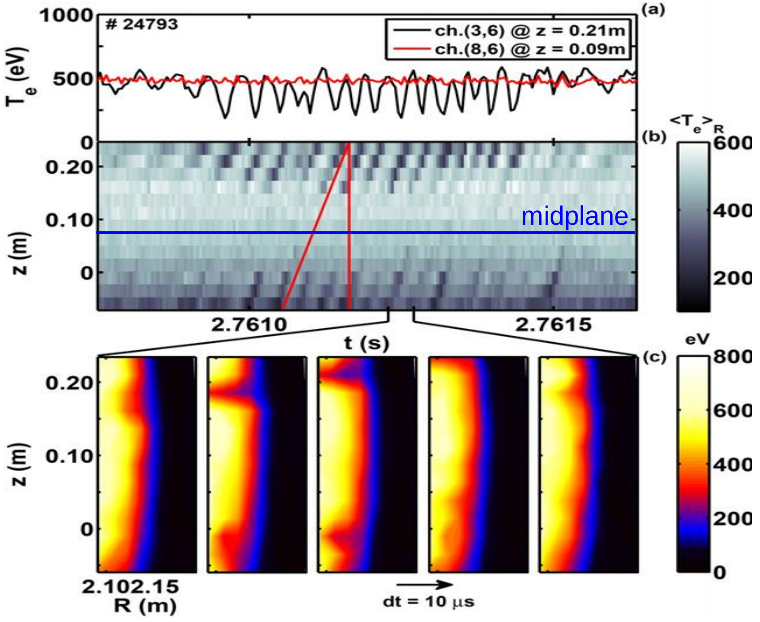

J. Boom *et al*, NF **51** 103039 (2011)
P. Manz *et al*, PPCF **56** 035010 (2014)

Gyrokinetic analysis reveals four main instabilities during different phases of ELM cycle

- Local linear gyrokinetic simulations of inter-ELM pedestal profile evolution using GENE*
- In early phase of ELM cycle (iii):
  drift waves dominate, L_{ne} at critical value
- ∇T_e achieves critical value early in ELM cycle (iv), simultaneous appearance of MTMs and ETGs

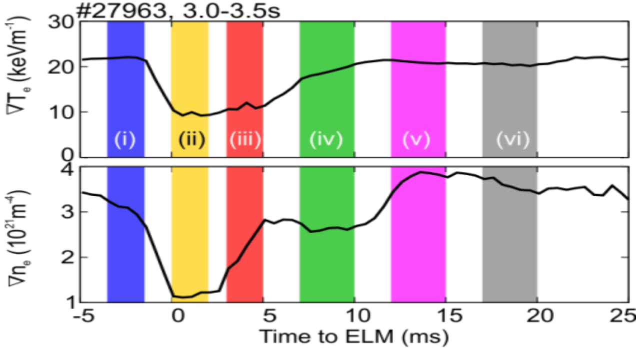

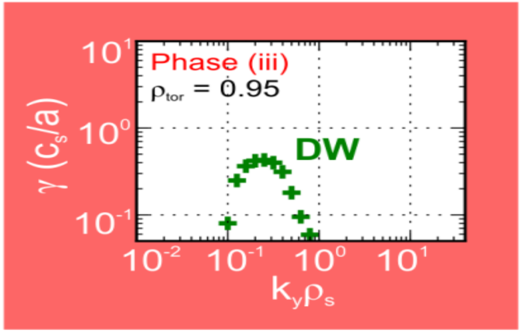

See D. Hatch et al, PD/P5-4

*F. Jenko *et al*, PoP **7** 1904 (2000)

D. Hatch *et al*, to be submitted

Gyrokinetic analysis reveals four main instabilities during different phases of ELM cycle

- Local linear gyrokinetic simulations of inter-ELM pedestal profile evolution using GENE*
- In early phase of ELM cycle (iii):
  drift waves dominate, L_{ne} at critical value
- ∇T_e achieves critical value early in ELM cycle (iv), simultaneous appearance of MTMs and ETGs
- Final pre-ELM state (i):
  'zoo' of modes → at small scale structures ETGs are dominant, at large scales MTMs and KBMs (10-20% increase in β sufficient to excite KBMs)
- Simulations consistent with KBM-constrained pedestal evolution

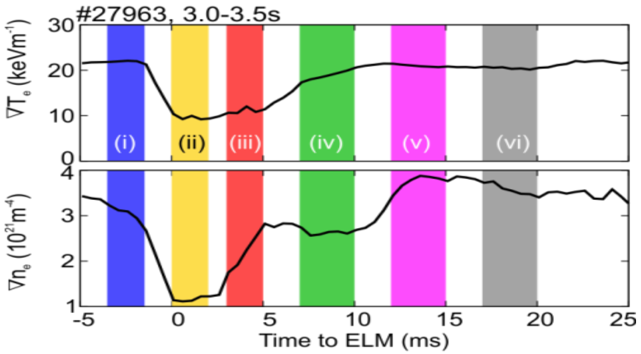

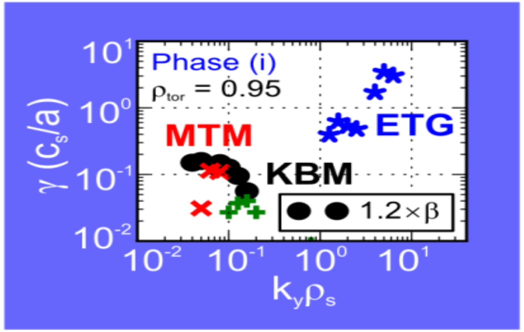

See D. Hatch et al, PD/P5-4

*F. Jenko *et al*, PoP **7** 1904 (2000)

D. Hatch *et al*, to be submitted

Summary and Conclusions

- Density build-up after L-H transition can be modelled with purely diffusive edge barrier (if pinch, then small ~0.4 m/s)
- Edge E_r, in-out impurity asymmetries and current density are consistent with neoclassical theory
- Inter-ELM pedestal evolution shows different phases:
  - Early phase: ∇n_e driven drift waves
  - Before ELM: KBMs, ETGs in gradient region limit transport, MTMs on pedestal shoulder, pedestal widens and stability boundary moves closer to operational point
- Critical pedestal not always predicted by ideal linear MHD
  - Possible reasons: resistivity, nonlinear coupling of modes

Backup slides

Neoclassical pedestal poloidal rotation observed in banana to PS regimes

- Analysis extended to low collisionality regime
- Good agreement found in all cases with ν^* varying from 0.18-12
- Neoclassical main ion poloidal rotation flips sign in banana regime
- Measured edge toroidal rotation ($\rho_{pol} \approx 0.97$) changes from co- to counter-current

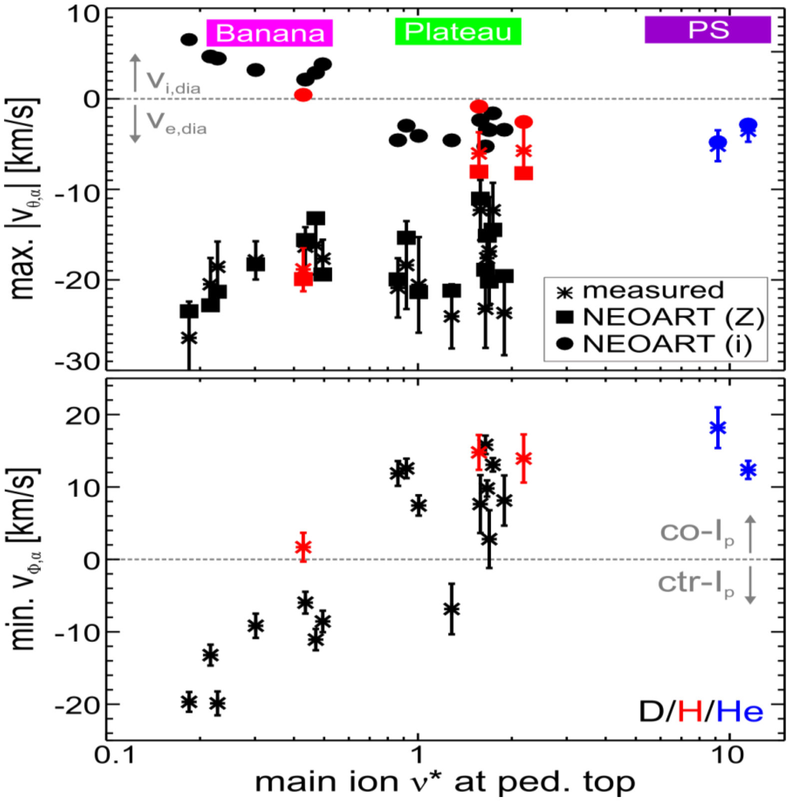

v_θ described by neoclassical theory

- comparison of measured and simulated impurity (N) v_θ in D plasma using analytic model[1], NEOART[2], NEO[3], HAGIS[4]

- all models agree with experiment

- in H-mode sign and magnitude of neocl. v_θ consistent with measurements[5]

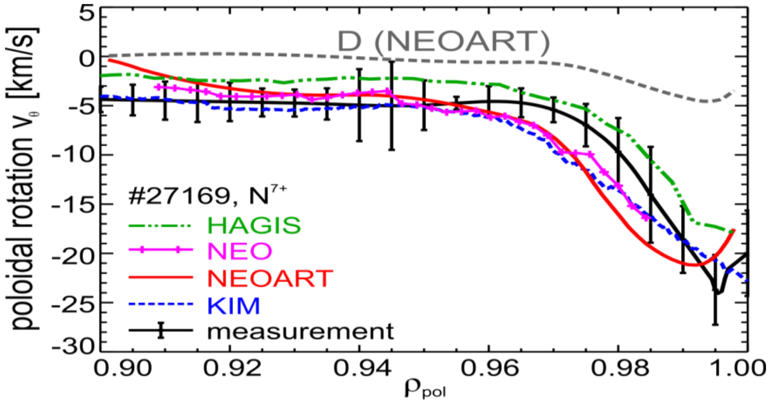

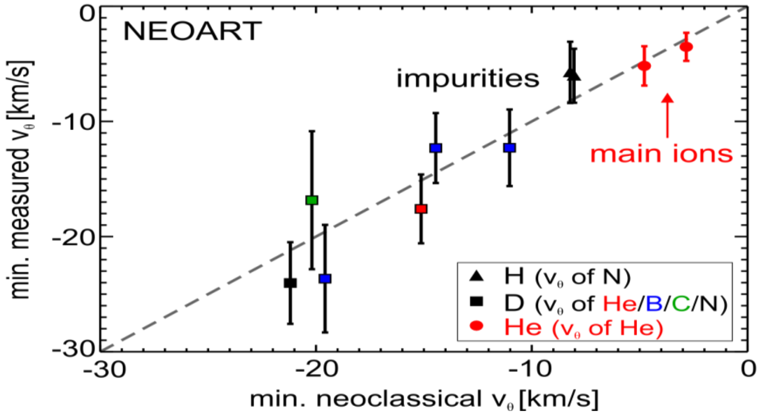

[1] Y. B. Kim *et al*, Phys. Fluids B **3** (8), 2050 (1991)
[2] A. G. Peeters *et al*, PoP **7** (1), 268 (2000)
[3] E. A. Belli *et al*, PPCF **50**, 095010 (2008)
[4] S. D. Pinches *et al*, Comp. Phys. Comm. **111**, 133 (1998)
[5] E. Viezzer *et al*, NF **54** 012003 (2014)

In some cases quantitative agreement with PB theory observed

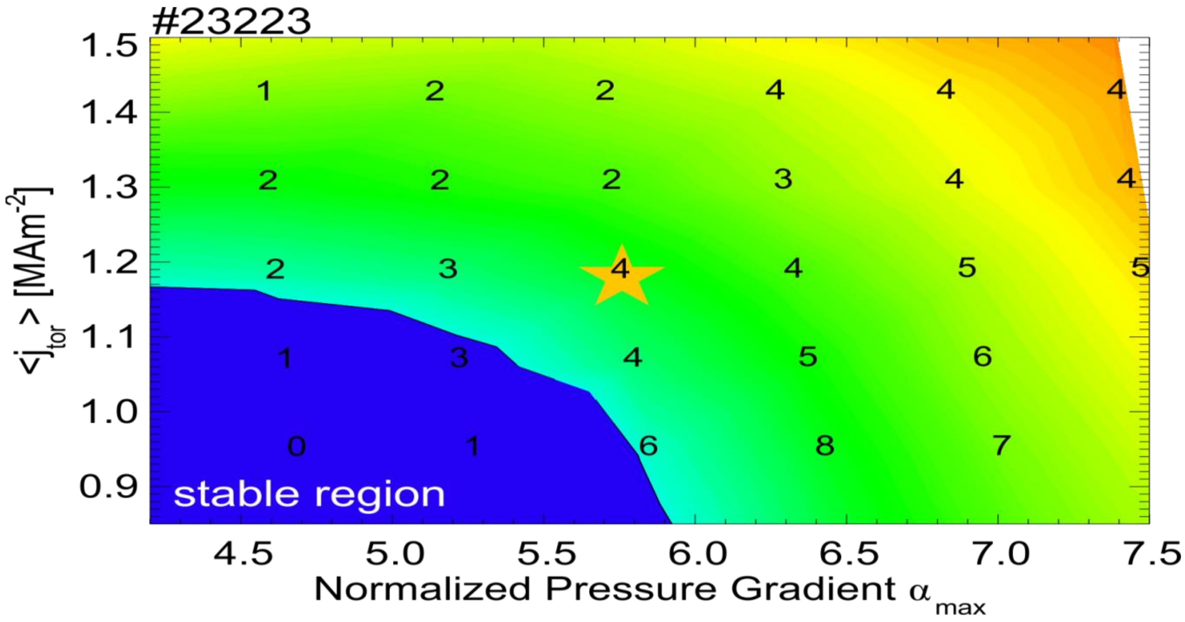

Comparison of ion Larmor radius and gradient scale lengths in the pedestal

- Ion Larmor radius at the plasma edge ~10 lower than L_{Ti}

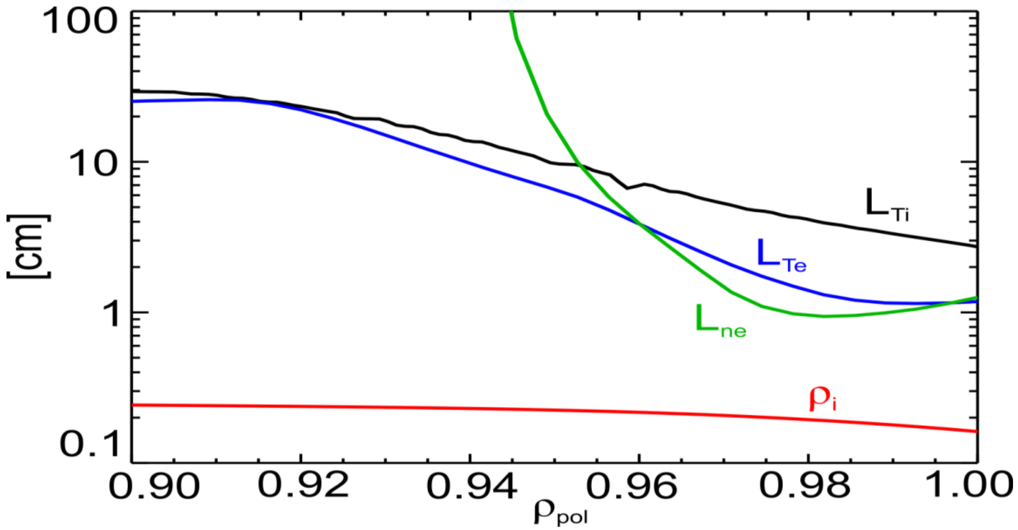

Comparison of ion Larmor radius and gradient scale lengths in the pedestal

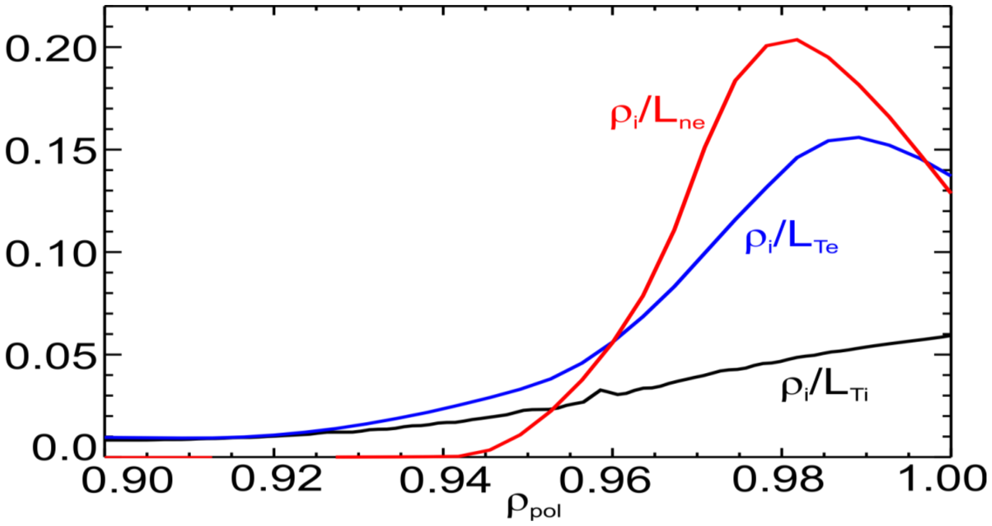

Peeling-ballooning stability analysis during ELM cycle

- Before ELM crash (i)+(vi): j and ∇p constant
- After ELM crash (ii): j and ∇p recover gradually as ∇n_e builds up (iii), followed by build-up of ∇T_e (iv)
- Towards end of ELM cycle (v):
  j saturates as soon as ∇p saturates → pedestal is clamped at critical gradient before ELM crash
- Towards end of ELM cycle stability boundary moves closer to op. point because pedestal width grows
- Final ELM trigger not determined by linear MHD stability alone (op. point ~30% lower than boundary)
- Other cases do show agreement with PB model

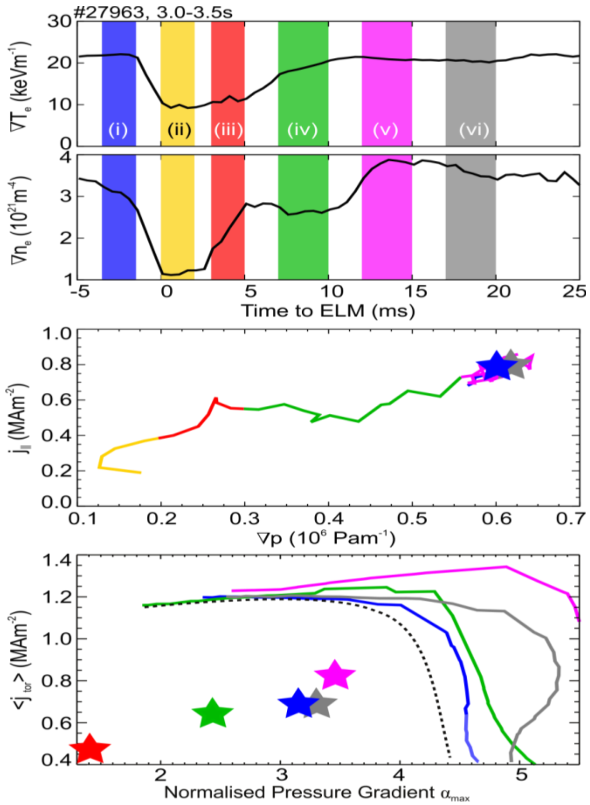

P. B. Snyder *et al*, PoP 19 056115 (2012) D. Dickinson *et al*, PPCF **53** 115010 (2011) A. Burckhart, PhD thesis, LMU Munich 2013

ECE-Imaging indicates presence of MTMs on pedestal shoulder

- For slow type-I ELMs 2D ECEI reveals occurrence of off-midplane T_e fluctuations on pedestal top, followed by mode at onset of ELM crash
- Both modes move in $v_{e,dia}$, substantiated by cross-correlation of two neighbouring channels, frequency ~ 20-60 kHz
- Velocimetry: determination of radial propagation velocity from 2D array of ECEI
- Cross-phase between $\tilde{T}_e$ and $\tilde{v}_r$ ~ $\pi/2$ at ρ_{pol}~0.95 → points to MTMs on pedestal shoulder

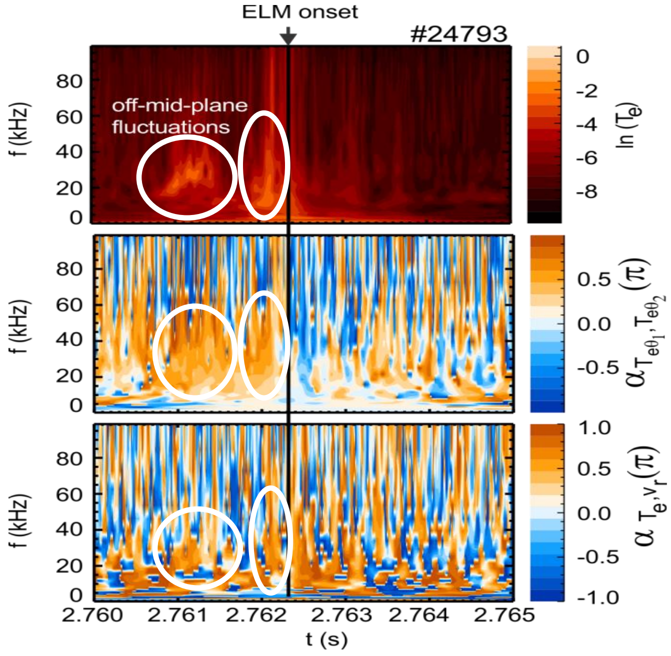

P. Manz *et al*, PPCF **56** 035010 (2014)

Experimental evidence for MTMs on pedestal shoulder from ECEI

- For slow type-I ELMs 2D ECEI reveals occurrence of off-midplane T_e fluctuations on pedestal top, followed by mode at onset of ELM crash
- Both modes move in $v_{e,dia}$, substantiated by cross-correlation of two neighbouring channels, frequency ~ 20-60 kHz
- Velocimetry: determination of radial propagation velocity from 2D array of ECEI
- Cross-phase between $\tilde{T}_e$ and $\tilde{v}_r$ ~ $\pi/2$ at ρ_{pol}~0.95 → points to MTMs on pedestal shoulder

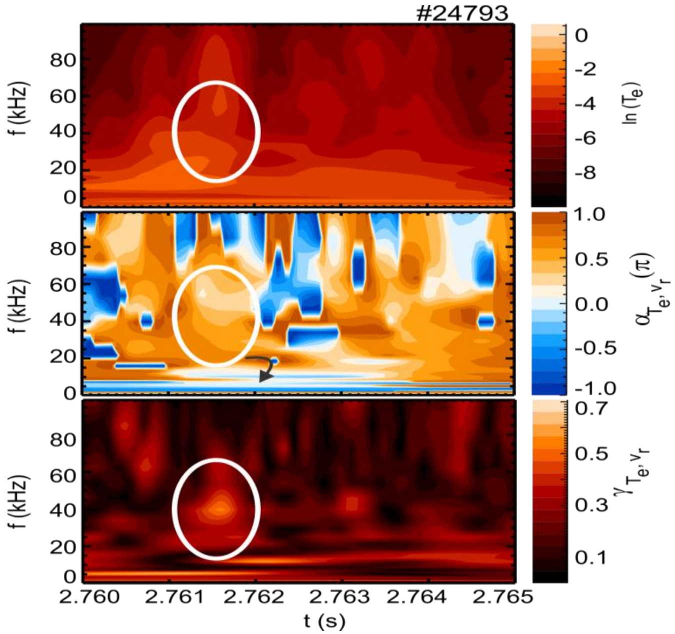

P. Manz *et al*, PPCF **56** 035010 (2014)

Asymmetry in flow structure consistent with divergence-free flows

- HFS/LFS CXRS demonstrate existence of in-out impurity density asymmetry in ETB → asymmetric flow structure on flux surface consistent with $\nabla\cdot(n_\alpha v_\alpha) = 0$

- Comparison to fluid model shows that friction and poloidal centrifugal force are dominant driving terms close to LCFS

- Observed flow structure can be reproduced quantitatively by model when including finite poloidal flow of main ions

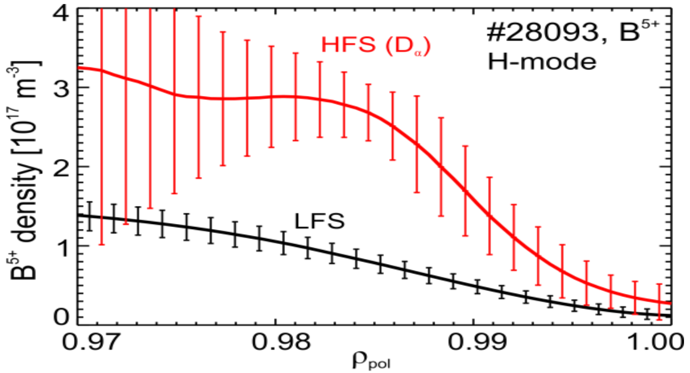

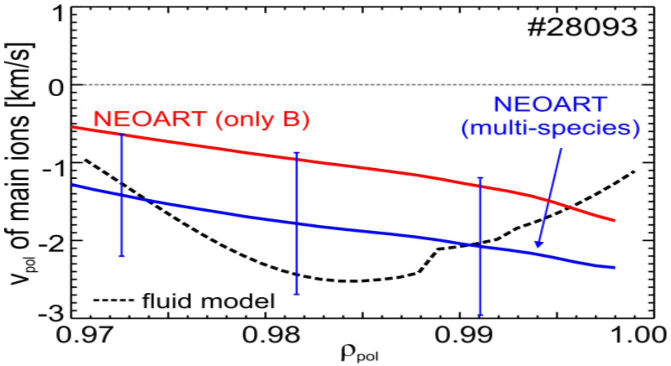

E. Viezzer *et al*, PPCF **55** 124037 (2013)

Asymmetry in flow structure consistent with divergence-free flows

- HFS/LFS CXRS demonstrate existence of in-out impurity density asymmetry in ETB → asymmetric flow structure on flux surface consistent with $\nabla\cdot(n_\alpha v_\alpha) = 0$

- Fluid model based on parallel momentum balance including all terms → friction and poloidal centrifugal force (CF) are dominant driving terms close to LCFS

- Only small influence on neoclassical impurity transport (v/D)

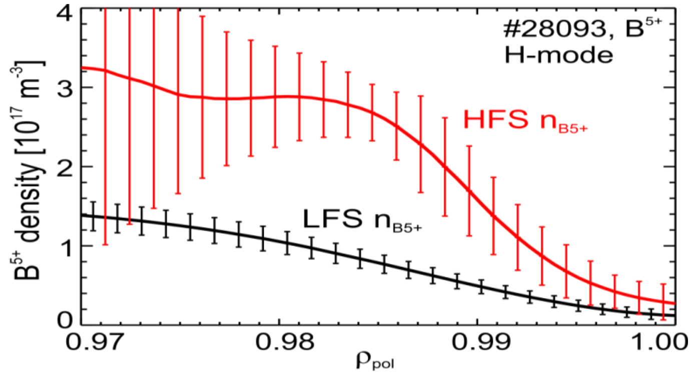

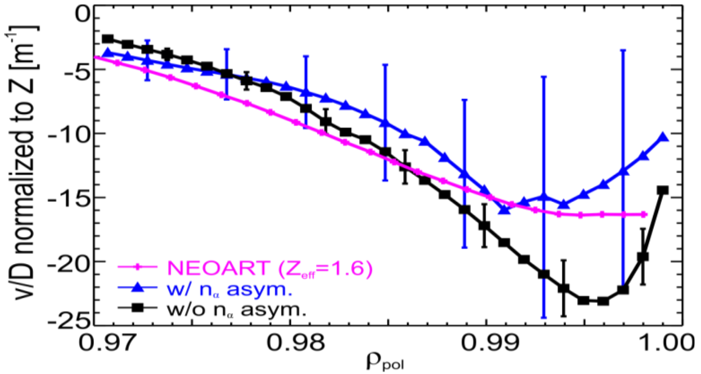

E. Viezzer *et al*, PPCF **55** 124037 (2013)
T. Pütterich *et al*, NF **52** 083013 (2012)

ASDEX Upgrade

Why does asymmetric n_α arise?

IPP

- study possible mechanism that could generate poloidal n_α asymmetry using parallel momentum transport equation (steady state $\partial/\partial t = 0$)

$$\vec{B}\cdot\vec{\nabla}\left(\boxed{\frac{u_\theta{}^2 B^2}{2B_\theta{}^2}} - \boxed{\frac{\Omega^2 R^2}{2}}\right) + \boxed{\vec{B}\cdot\frac{\vec{\nabla}P}{n_\alpha}} + \boxed{\vec{B}\cdot\frac{\vec{\nabla}\cdot\overleftrightarrow{\Pi}}{n_\alpha}} + \boxed{Z_\alpha\vec{B}\cdot\vec{\nabla}\phi} = -\nu_{\alpha i}\vec{B}\cdot\left(\boxed{\vec{u}_{\parallel,\alpha} - \vec{u}_{\parallel,i}} + \boxed{\Delta Q_\parallel}\right)$$

pol. CF | tor. CF | pressure drive | stress tensor | electric drive | friction | thermal force

- solve for n_α and connect flows to n_α via divergence-free flow condition

- predictions based on fluid model[1] and kinetic approach[2]
  - fluid model solves || momentum balance analytically
  - drift-orbit code (HAGIS[3]) includes MC pitch angle collision model[4]
    → calculation of NC transport

[1] E. Fable *et al* (in preparation)
[2] A. Bergmann *et al* (in preparation)
[3] S. D. Pinches *et al*, CPC **111** 133 (1998)
[4] A. Bergmann *et al*, PoP **8** 5192 (2000)

ASDEX Upgrade

Kinetic and fluid models predict similar flow profiles

- parallel and poloidal impurity flows agree when same input parameters are applied (main ion dynamics)
- separation of parallel flows and difference in magnitude of pol. flows arise due to n_α asymmetry
- qualitative agreement with measurement
- however $\Delta v_{||,\alpha} = v^{HFS}_{||,\alpha} - v^{LFS}_{||,\alpha}$ larger in experiment

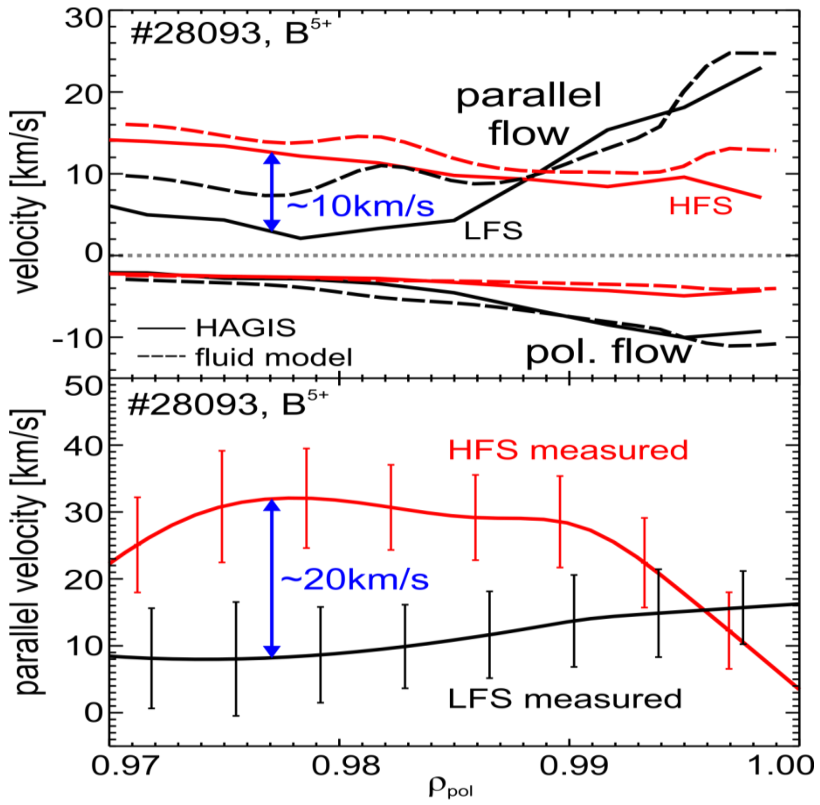

Measured parallel impurity flows are in good agreement with theoretical predictions

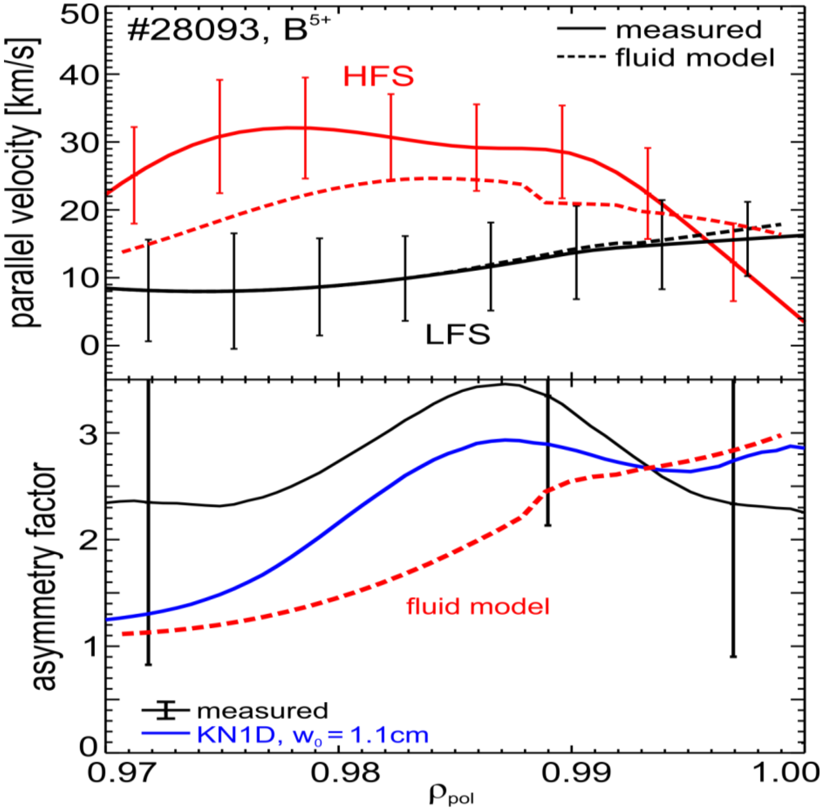

- flow structure and asymmetry factor reproduced by model (input: measured LFS flows)

E. Fable *et al* (in preparation)

Measured parallel impurity flows are in good agreement with theoretical predictions

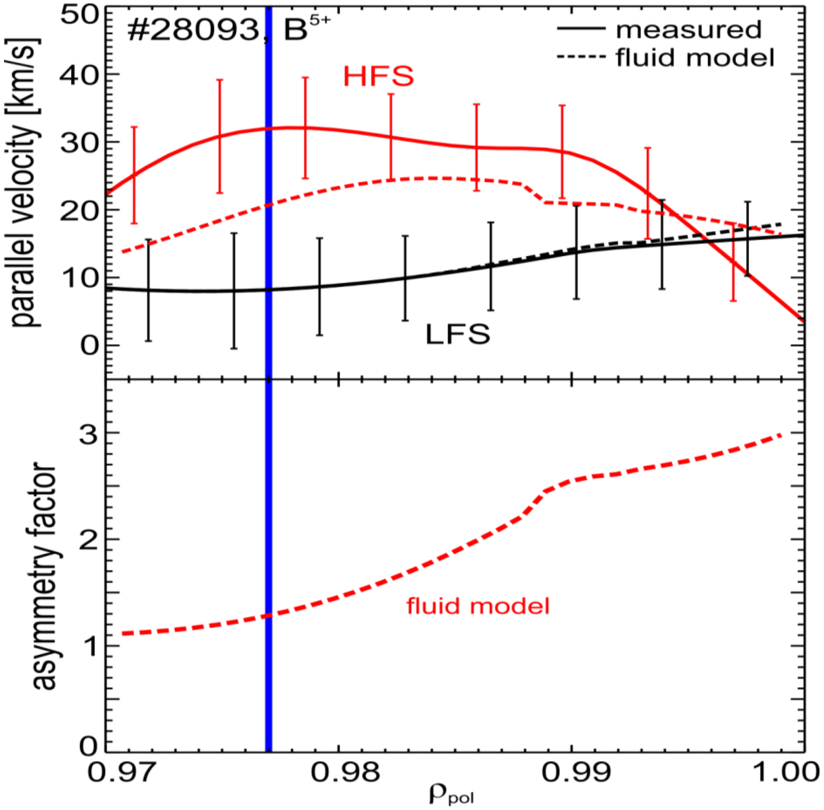

- flow structure and asymmetry factor reproduced by model (input: measured LFS flows)

E. Fable *et al* (in preparation)

- max. $\Delta v_{||,\alpha}$ for low n_α asymmetry

Measured parallel impurity flows are in good agreement with theoretical predictions

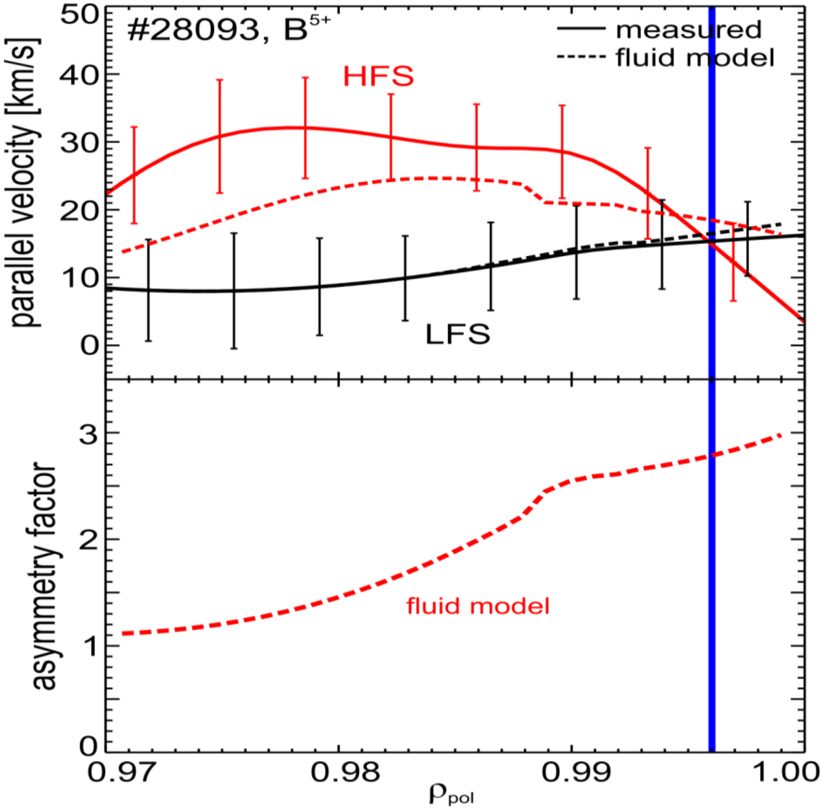

- flow structure and asymmetry factor reproduced by model (input: measured LFS flows)

E. Fable *et al* (in preparation)

- max. $\Delta v_{||,\alpha}$ for low n_α asymmetry

- crossing point in $v_{||,\alpha}$ for high n_α asymmetry

Poloidal centrifugal force term increases towards LCFS

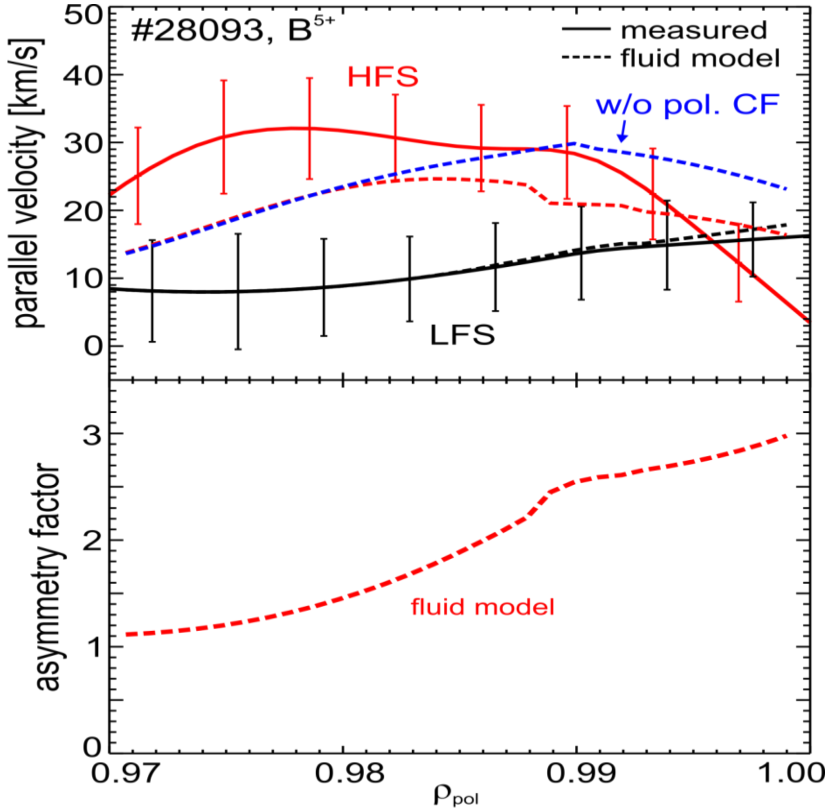

- flow structure and asymmetry factor reproduced by model (input: measured LFS flows)

  E. Fable *et al* (in preparation)

- max. $\Delta v_{||,\alpha}$ for low n_α asymmetry
- crossing point in $v_{||,\alpha}$ for high n_α asymmetry
- considerable contribution from pol. CF near separatrix (high $v_{pol,\alpha}$)

Predicted poloidal main ion flow of ~2km/s consistent with neoclassical theory

- measured impurity flows → indirect information on main species
- fluid model predicts main ion poloidal flow of ~2 km/s
- in good agreement with standard neoclassical prediction using NEOART ($Z_{eff} \approx 1.6$)

A. Peeters *et al*, PoP **7** 268 (2000)

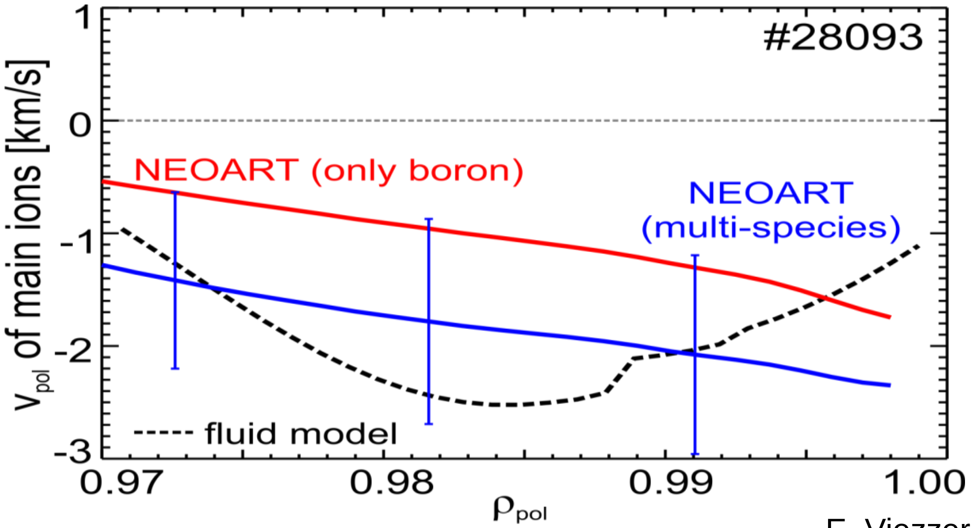

E. Viezzer *et al*, PPCF **55** 124037 (2013)

HFS and LFS CXRS enables localized E_r and in-out impurity asymmetry measurements

- Toroidal beam-based edge CXRS system extended by poloidal view
  → enables localized v_θ measurement
  → all ingredients for E_r using radial impurity force balance equation

$$\boxed{E_r = \frac{1}{n_\alpha Z_\alpha e}\frac{\partial p_\alpha}{\partial r} - v_{\theta,\alpha}B_\phi + v_{\phi,\alpha}B_\theta}$$

- Installation of toroidal and poloidal views at HFS of AUG allows for measurement of T_α, n_α, $v_{rot,\alpha}$ and E_r at two poloidal locations → poloidal impurity asymmetry studies

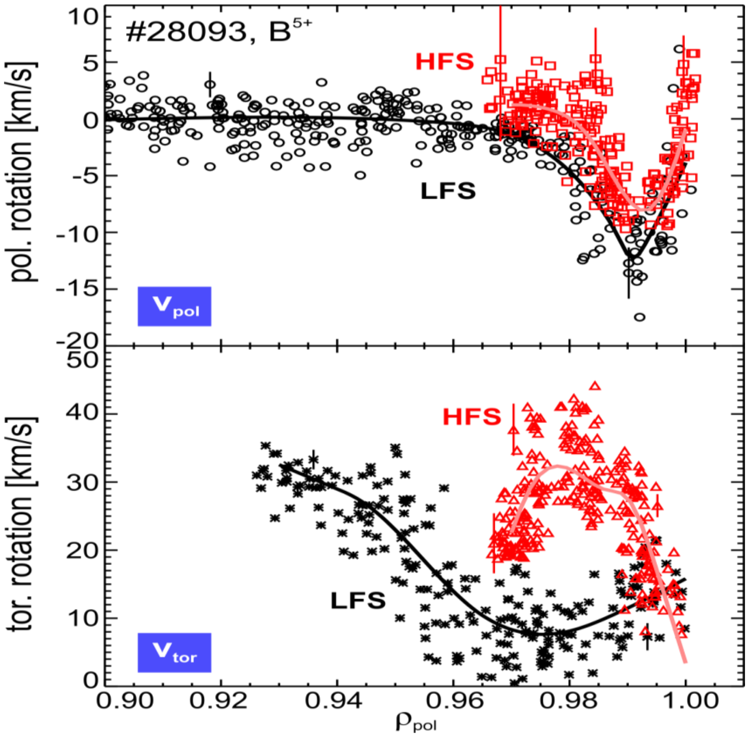

E. Viezzer *et al*, RSI **52** 123014 (2012)
T. Pütterich *et al*, NF **52** 083013 (2012)

Forward modelling of ECE radiation transport reveals steeper edge ∇T_e

- Reliable edge ∇T_e by forward modelling of ECE radiation transport (ECFM) using Bayesian probability theory
  → shine-through peak is reproduced
  → actual ∇T_e steeper

- Joint analysis of n_e and T_e with full probabilistic model including physical
  and statistical description of an integrated set of different diagnostics (ECE, LIB, DCN, TS)

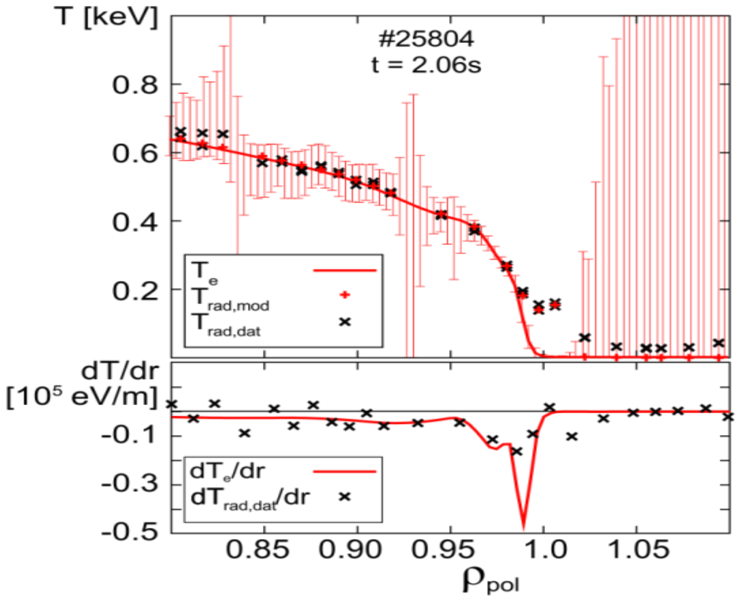

S. K. Rathgeber *et al*, PPCF **55** 025004 (2013)
R. Fischer *et al*, FST 58 675 (2010)

Determination of edge current density using pressure constrained equilibrium solver CLISTE

ASDEX Upgrade

- For axis-symmetry equilibrium determined by Grad-Shafranov equation
  AUG: Grad-Shafranov solver CLISTE

- External magnetic field pick-up coils sensitive to current at X-point

- Knowledge of poloidal SOL currents and kinetic profiles provide valuable constraints on j profile

- Including additional constraints results in narrower and more peaked j

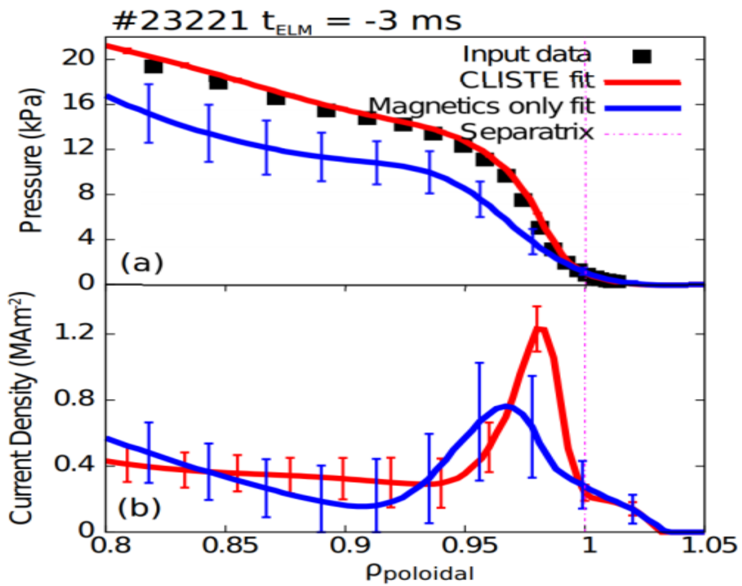

CLISTE standard = magnetics only
CLISTE with pressure constraint

P. J. McCarthy *et al*, PPCF (2012)
M. G. Dunne *et al*, NF **52** 123014 (2012)

Edge current density is neoclassical

- Assume current driven by neoclassical bootstrap* and Ohmic current, neglect fast ion current, $\langle j_{PS} \cdot B \rangle = 0$

$$\boxed{\langle j_{\mathrm{neo}} \cdot B \rangle = \langle j_{\mathrm{boot}} \cdot B \rangle + \langle j_{\mathrm{Ohm}} \cdot B \rangle}$$

- Comparison of edge current density to neoclassical prediction shows quantitative agreement

- Position and peak match, good agreement also during ELM cycle

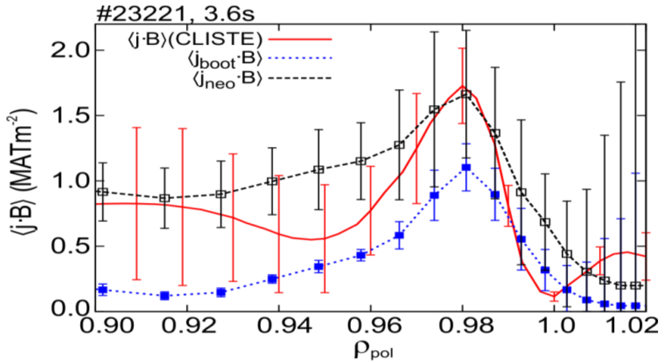

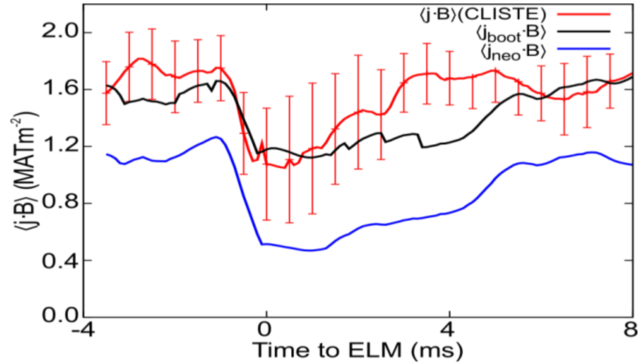

*O. Sauter *et al*, PoP **6** 2834 (1999)

M. G. Dunne *et al*, NF **52** 123014 (2012)

Edge current density is neoclassical

- Assume current driven by neoclassical bootstrap* and Ohmic current, neglect fast ion current, $\langle j_{PS} \cdot B \rangle = 0$

$$\boxed{\langle j_{\text{neo}} \rangle = \langle j_{\text{boot}} \rangle + \langle j_{\text{Ohm}} \rangle}$$

- Comparison of edge current density to neoclassical prediction shows quantitative agreement

- Position and peak match, good agreement also during ELM cycle

- CXRS data indicates faster T_i recovery after ELM crash → important contribution of T_i for neoclassical current

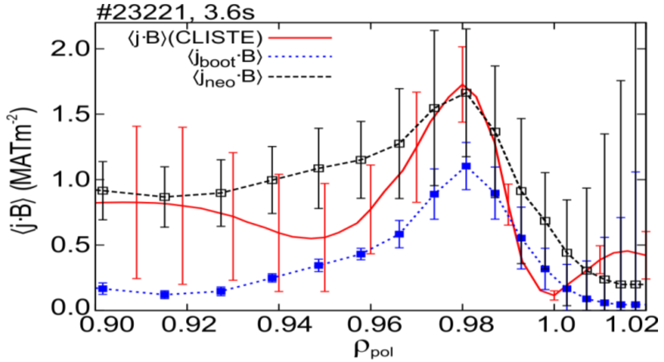

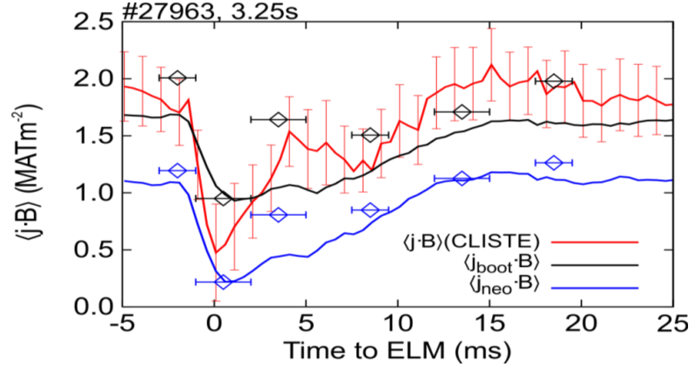

O. Sauter *et al*, PoP **6** 2834 (1999)

M. G. Dunne *et al*, NF **52** 123014 (2012)

Density build-up after L-H transition depends on gas reservoirs in divertor

- Modeling of the density build-up after L-H transition using ASTRA*
- Is the particle ETB due to a particle pinch v_e or a reduction of diffusion D?
- Analysis of ECRH induced H-mode phases
- Complete n_e profile (IDA)

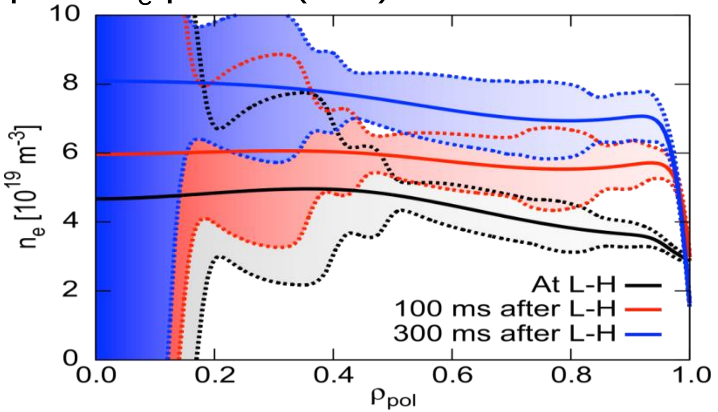

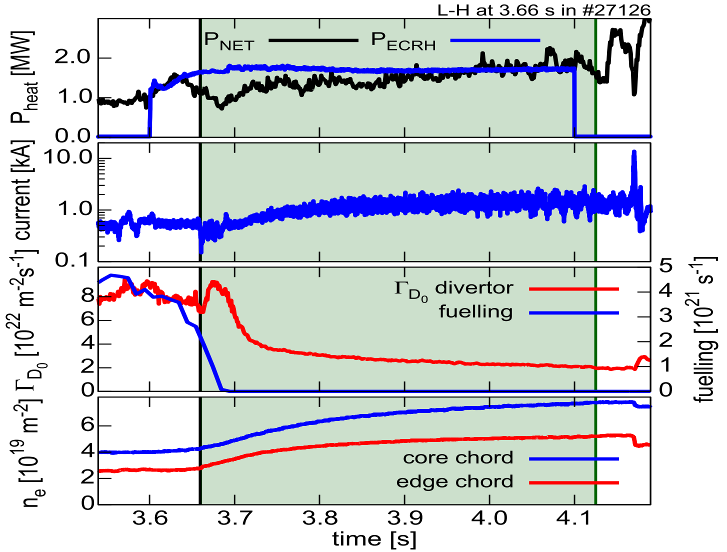

M. Willensdorfer *et al*, NF **53** 0930201 (2013)

*G. V. Pereverzev *et al*, IPP 5/42 (1991)

Particle source

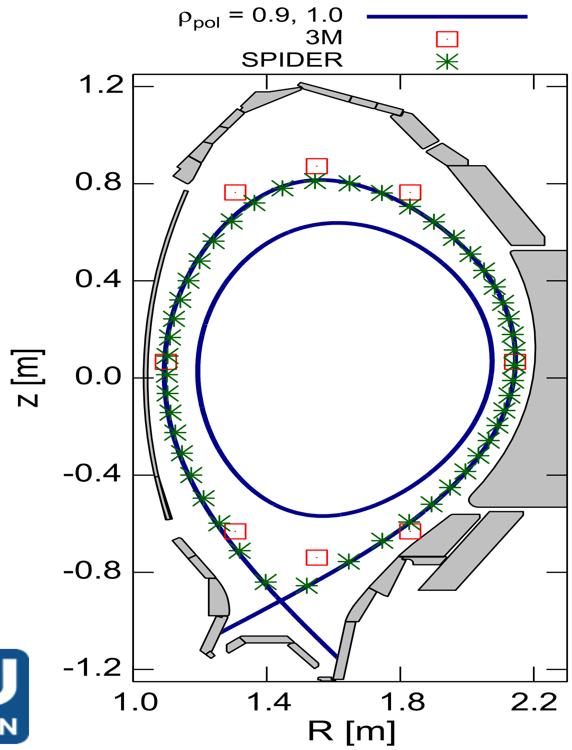

Using NEUT and following assumptions:

- Neutral gas density of incoming neutrals (n_0 @ LCFS) constant in time
- Temperature of incoming neutrals has one value (3eV, Franck-Condon), NEUT solves kinetic eq. for neutral distribution function
- 3-moment solver is used for the equilibrium (no X-point geometry)

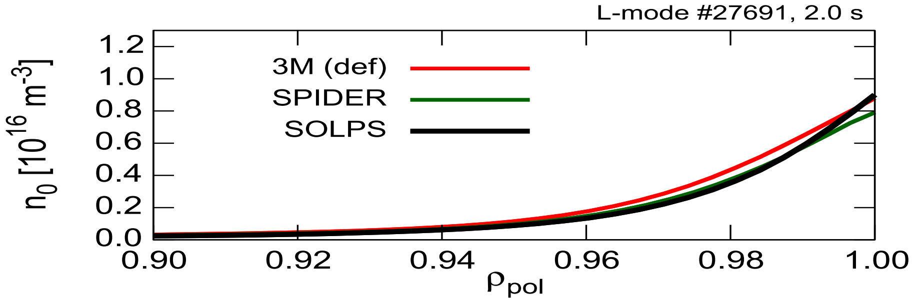

[M. Willensdorfer, submitted to NF]

Purely diffusive ETB delivers reasonable results

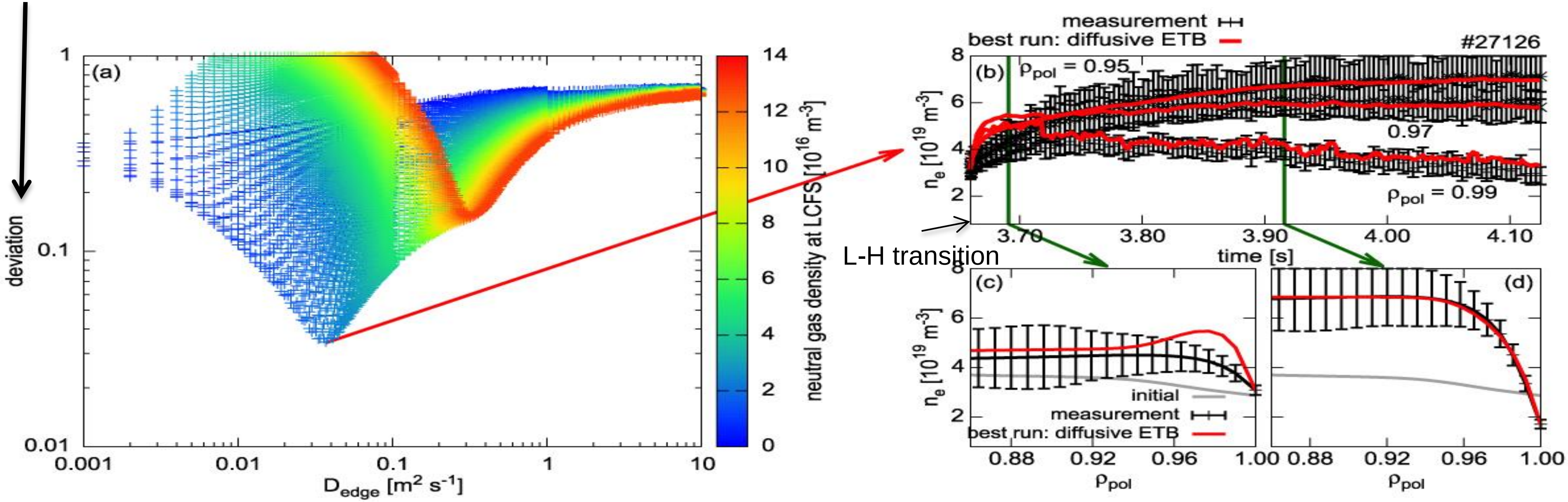

Reasonable results assuming $n_0 = 1.6\ 10^{16}\ m^{-3}$ and $D_{edge} \sim 0.037\ m^2/s$

The initial increase more smooth in measurements than in modeling.

[M. Willensdorfer, submitted to NF]

ASDEX Upgrade

Pinch cannot replace diffusive ETB

IPP

$$\frac{\partial n_e}{\partial t} + \frac{1}{r}\frac{\partial}{\partial r} r\left(- D\cancel{(r)}\,\frac{\partial n_e}{\partial r} + v_e n_e\right) = S$$

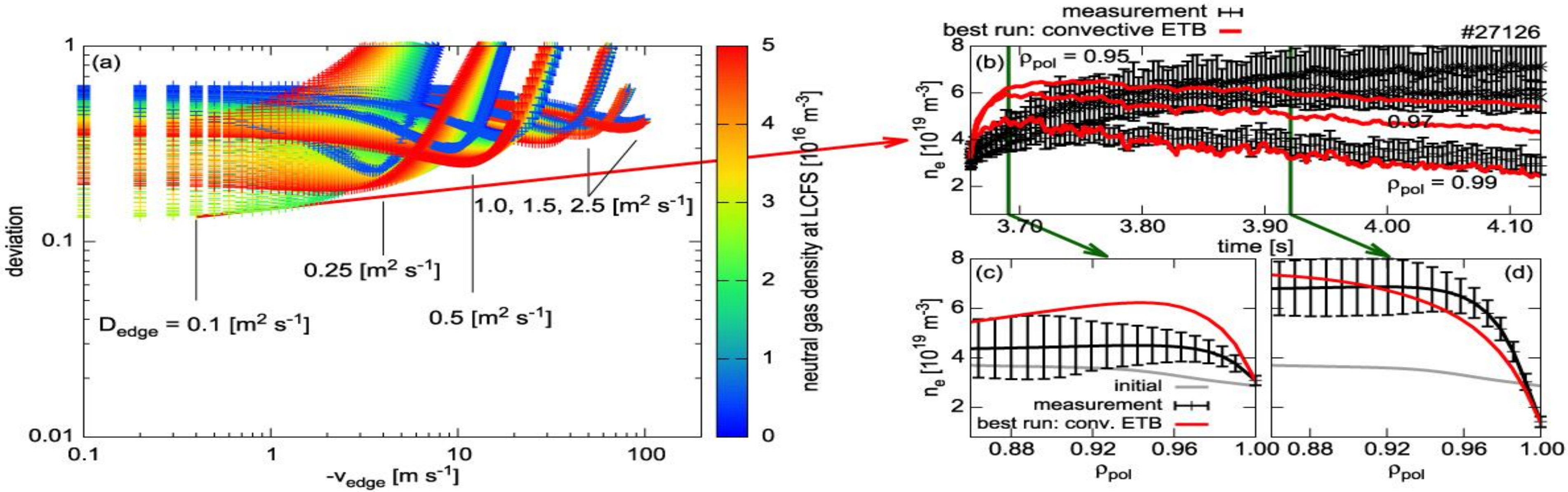

Deviation always > 10%!!

Transport barrier in D cannot be replaced by particle pinch!

[M. Willensdorfer, submitted to NF]

Small pinch delivers slightly better results

$$\frac{\partial n_e}{\partial t} + \frac{1}{r}\frac{\partial}{\partial r} r\left(- D\frac{\partial n_e}{\partial r} + v_e n_e\right) = S$$

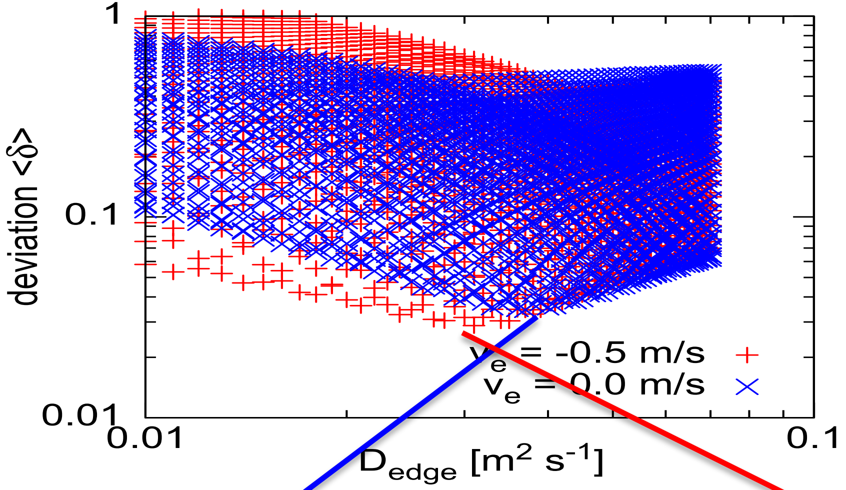

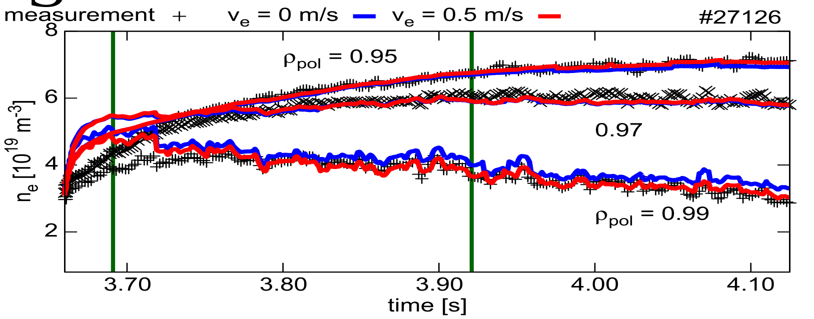

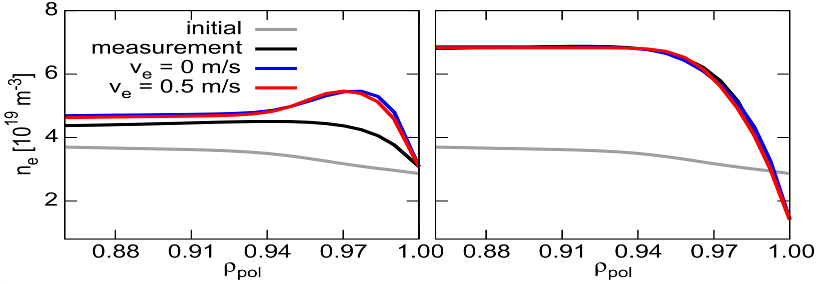

$n_0 = 1.6\ 10^{16}\ m^{-3}$

$n_0 = 1.1\ 10^{16}\ m^{-3}$

Small particle pinch 0.5 m/s betters the result.

The pinch replaces the source.

Range estimation pinch (zero source)

$$\frac{\partial n_e}{\partial t} + \frac{1}{r}\frac{\partial}{\partial r} r\left(-D\frac{\partial n_e}{\partial r} + v_e n_e\right) = \cancel{S}$$

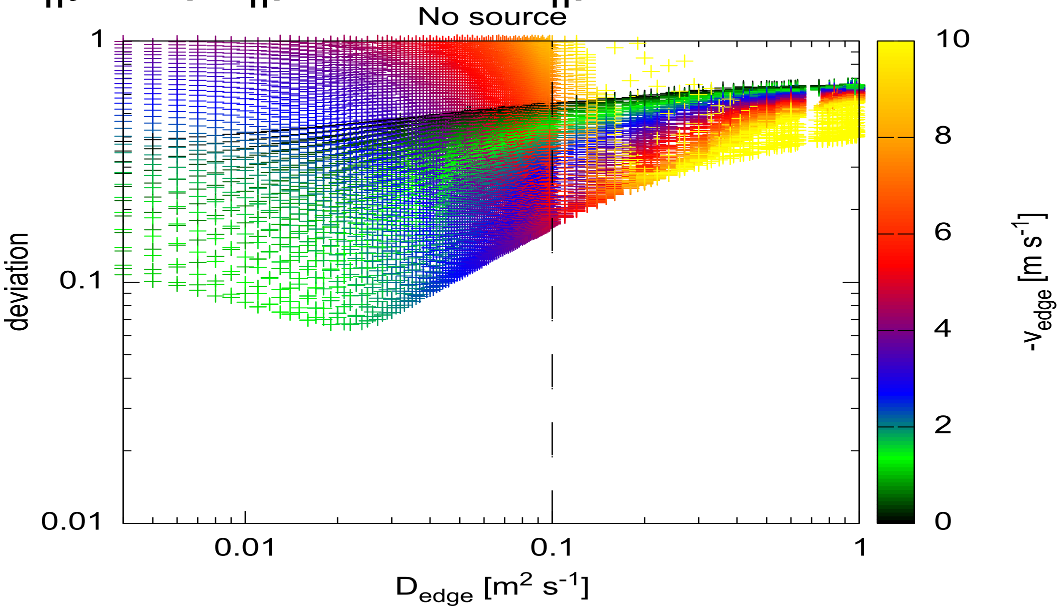

Particle pinch in the presence of e.g. D_{edge}~ 0.1 m^2/s is maximal 5 m/s.

[M. Willensdorfer, submitted to NF]

Density build-up can be reproduced by assuming purely diffusive ETB

- Diffusive ETB is needed to reproduce n_e build-up after L-H transition (D_{edge} ~ 0.037 m^2/s)
- Particle pinch cannot replace diffusive ETB
- Small pinch (~ 0.4 m/s) in addition to diffusive ETB enhances simulation
- Range of possible pinch is 0-5 m/s

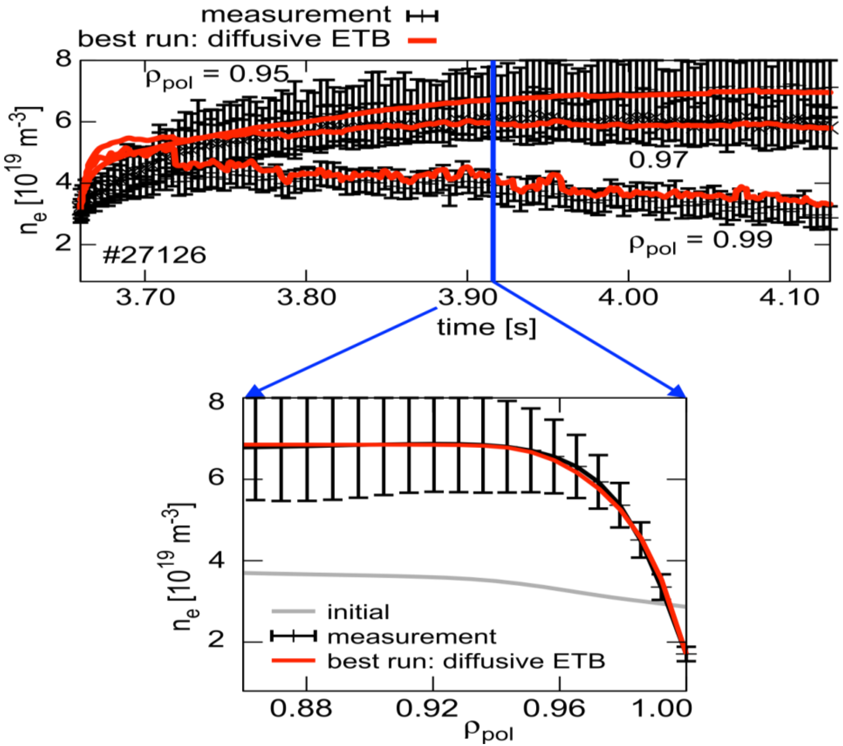

M. Willensdorfer *et al*, NF **53** 0930201 (2013)